


A review of the LATEX project: mesoscale to submesoscale processes in a coastal environment

Anne A. Petrenko¹  · Andrea M. Doglioli¹ · Francesco Nencioli² · Marion Kersalé³ · Ziyuan Hu⁴ · Francesco d'Ovidio⁵

Received: 7 October 2016 / Accepted: 10 February 2017
© Springer-Verlag Berlin Heidelberg 2017

Abstract The main objective of the LAgrangian Transport EXperiment (LATEX) project was to study the influence of coastal mesoscale and submesoscale physical processes on circulation dynamics, cross-shelf exchanges, and biogeochemistry in the western continental shelf of the Gulf of Lion, Northwestern Mediterranean Sea. LATEX was a five-year multidisciplinary project based on the combined analysis of numerical model simulations and multi-platform field experiments. The model component included a ten-year realistic 3D numerical simulation, with a 1 km hor-

izontal resolution over the gulf, nested in a coarser 3 km resolution model. The *in situ* component involved four cruises, including a large-scale multidisciplinary campaign with two research vessels in 2010. This review concentrates on the physics results of LATEX, addressing three main subjects: (1) the investigation of the mesoscale to submesoscale processes. The eddies are elliptic, baroclinic, and anticyclonic; the strong thermal and saline front is density compensated. Their generation processes are studied; (2) the development of sampling strategies for their direct observations. LATEX has implemented an adaptive strategy Lagrangian tool, with a reference software available on the web, to perform offshore campaigns in a Lagrangian framework; (3) the quantification of horizontal mixing and cross-shelf exchanges. Lateral diffusivity coefficients, calculated in various ways including a novel technique, are in the range classically encountered for their associated scales. Cross-shelf fluxes have been calculated, after retrieving the near-inertial oscillation contribution. Further perspectives are discussed, especially for the ongoing challenge of studying submesoscale features remotely and from *in situ* data.

Responsible Editor: Simon Ruiz

This article is part of the Topical Collection on the *48th International Liège Colloquium on Ocean Dynamics, Liège, Belgium, 23-27 May 2016*

✉ Anne A. Petrenko
anne.petrenko@mio.osupytheas.fr

¹ Aix Marseille Université, Université de Toulon, CNRS, IRD, Mediterranean Institute of Oceanography (MIO), Marseille, France

² Remote Sensing Group, Plymouth Marine Laboratory, Plymouth, UK

³ Department of Oceanography, Marine Research Institute, University of Cape Town, Rondebosch, South Africa

⁴ Jiaozhou Bay Marine Ecosystem Research Station, Institute of Oceanology, Chinese Academy of Sciences, Qingdao, China

⁵ Sorbonne Université (UPMC, Paris 6)/CNRS/IRD/MNHN, Laboratoire d'Océanographie et du Climat (LOCEAN), Institut Pierre Simon Laplace (IPSL), Paris, France

Keywords Mesoscale · Submesoscale · Lagrangian · Gulf of Lion · Northwestern mediterranean sea · Cross-shelf flux

1 Introduction

Coastal waters, in spite of their small surfaces and volumes (8 and 0.05% of the global ocean, respectively), are currently the object of crucial questions. This environment is the link between the continents, highly impacted by human presence and activities (40% of the world population lives

less than 100 km from the coast) and the ocean, one of the main regulators of the global thermal and biogeochemical cycles. The coastal zone is usually characterized by high biological productivity due to a large availability in nutrients coming from human and river inputs. Thus, coastal areas contribute to an important part of the carbon sequestration in the ocean and play a key role in climate change. Moreover, coastal dynamics has strong ecological repercussions, such as the regulation of biogeochemical cycles through local circulation and cross-shelf exchanges, as well as the dispersion of larvae and pollutants through current advection. Coastal physical processes also influence higher trophic levels having, for example, repercussions for fisheries. Their understanding is therefore of critical importance for sustainable management of the marine environment. Among coastal physical processes, mesoscale and submesoscale—hereafter referred to as (sub)mesoscale—processes have a particularly important role.

(Sub)mesoscale processes are ubiquitous in the open ocean, as well as in coastal waters. They have spatial scales of the order of few kilometers and temporal scales of days to weeks, hence they are typically localized and ephemeral. On one hand, mesoscale processes are generally produced by the instability of large-scale currents (McWilliams et al. 1983; Robinson 1983). They are in approximate geostrophic balance in the horizontal and hydrostatic balance in the vertical and are characterized by small Rossby and Froude numbers (Cushman-Roisin 1994). Thus, their dynamics are predominantly horizontal. Submesoscale processes, on the other hand, usually arise from instabilities in the mixed layer due to mesoscale-induced stirring, wind forcing, or a combination of the two (e.g., Thomas et al. 2008). They are characterized by $\mathcal{O}(1)$ Rossby and Richardson numbers. Thus, they are typically ageostrophic, and their dynamics markedly 3D. They can generate non negligible vertical motion and enhance local mixing. Hence, submesoscale processes can have an important biogeochemical impact by supplying nutrients both vertically and laterally (Moore II et al. 2007; Suthers et al. 2011; Mahadevan 2016). Length scales of mesoscale oceanic processes in coastal area are usually of $\mathcal{O}(10 - 100)$ km, while those of submesoscale processes of $\mathcal{O}(0.1 - 10)$ km. (Sub)mesoscale processes such as coastal eddies, fronts, and filaments are particularly important for coastal environments since they are key contributors to the energy budget, tracer transport, and biogeochemical cycles. This review focuses on the first two contributions.

Coastal eddies have generally been related to strong currents, mixed layer stratification and/or wind forcing (Mitchelson-Jacob and Sundby 2001), outflows of coastal waters (Crawford 2002; Di Lorenzo et al. 2005), flow instabilities along the continental slope (Melson et al. 1999; Flexas et al. 2002), topographic forcing (MacFadyen et al.

2008; Staneva et al. 2001), upwelling processes (MacFadyen and Hickey 2010) or transfers of energy from other eddies (Garreau et al. 2011).

Fronts are regions characterized by strong horizontal gradients of hydrographic properties (temperature, salinity, or both). Typically, the variations of a parameter across the front axis are an order of magnitude larger than changes of this parameter over the same distance on either side of the front. If the horizontal gradients of temperature and salinity are also associated with variations in density, the front is named a density front. While if the horizontal temperature gradient is balanced by that of salinity, so that the resulting cross-front density profile is almost constant, the front is called density-compensated. Fronts are linked to mesoscale dynamics because they are often created by mesoscale-induced stirring, although other processes can also generate them, e.g., tides, atmospheric forcing, freshwater inputs. They can also be linked to submesoscale dynamics, because the front's development often leads to, or is associated with the formation of 3D secondary ageostrophic circulation (Thomas et al. 2008; Capet et al. 2008b).

Coastal eddies and fronts have a strong influence on horizontal ocean mixing and, hence, could impact diffusivity. In the past, *in situ* estimates of lateral diffusivity at scales smaller than 100 km have been most commonly obtained from passive tracer (e.g., sulfur hexafluoride, SF_6) experiments. Such estimates are based on the hypothesis that, under local mesoscale stirring (which can be approximated, to a first order, as 2D and hence divergence-free), the width of the patch decreases until the effects of mesoscale stirring are balanced by smaller scale diffusion and an equilibrium is reached. Thus, lateral diffusivity can be computed by combining estimates of the strain rate (usually estimated from successive *in situ* mappings (Ledwell et al. 1998), or from the analysis of satellite imagery of surface tracers (Abraham et al. (2000)) with *in situ* measurements of the patch width. Lateral diffusivities computed using this approach range from 0.5 to 25 $m^2 s^{-1}$ for tracer filaments with widths between 1 and 10 km. At similar scales but in less energetic systems, lateral diffusivities have also been estimated by neglecting the strain and measuring the growth of the roughly circular tracer patch (e.g., the Santa Monica Basin Tracer Experiment (Ledwell and Watson 1991), and the BATRE experiment (Holtermann et al. 2012)). Following this method, the lateral diffusivities were of the order of 10 $m^2 s^{-1}$ for the interior of the two basins at scales on the order of 10 km.

Eddies and fronts can also have an important role on cross-shelf exchanges. In the last decades, cross-shelf exchanges have been the focus of several studies (Brink and Cowles 1991; Biscaye 1994; Huthnance et al. 2002; Johnson and Chapman 2011). Continental shelves are often bounded by strong large-scale (geostrophic)

currents flowing along the steep bathymetry of the shelf edge (Huthnance 1995). These tend to inhibit cross-shelf exchanges which, therefore, are mainly enabled by localized, mostly short-lived and predominantly ageostrophic events, such as internal tide breaking (Hopkins et al. 2012), Ekman transport (Kirincich and Barth 2009), dense shelf water cascading (Canals et al. 2006), eddies (Capet et al. 2008a; Nagai et al. 2015), mesoscale-stirred fronts (Ferrari 2011), and filaments (Nagai et al. 2015). Estimates of the net fluxes induced by these processes remain hard to quantify from *in situ* observations due to the temporal and spatial scales of the processes involved (Huthnance et al. 2009). In global models, the effect of (sub)mesoscale processes is still parametrized (e.g., eddy viscosities and diffusivities). Indeed, despite some recent advancements towards (sub)mesoscale resolving resolutions, they usually cannot properly resolve their associated dynamics. Nonetheless, (sub)mesoscale processes can now be accurately resolved by high-resolution regional numerical models. Therefore, the impact of these processes on coastal environments and cross-shelf exchanges has been investigated at the regional scale mainly through the analysis of numerical simulations with relatively rare concomitant observations for comparisons (Burchard et al. 2008; Capet et al. 2008a, b). For these reasons, direct observations of (sub)mesoscale processes still represent a key and much-needed component for the further advancement of both regional and global models.

The main objective of the LAGRangian Transport EXperiment (LATEX) project was to study the influence of coastal (sub)mesoscale physical processes on circulation dynamics, cross-shelf exchanges and biogeochemistry in the western continental shelf of the Gulf of Lion (GoL), Northwestern Mediterranean sea (Fig. 1). LATEX was a five-year (2007–2011) multidisciplinary project based on the combined analysis of numerical model simulations and multi-platform field experiments.

The GoL is a large continental shelf, approximately the shape of a semi-circle with a radius near 100 km, and a surface area of about 11000 km². The main forcings of the shelf circulation include the following: (i) the strong northerly and northwesterly continental winds (the Mistral and the Tramontane); (ii) the Northern Current (hereafter NC) which represents the northern branch of the large-scale cyclonic circulation of the western Mediterranean basin, flowing along the continental slope from the Ligurian Sea to the Catalan Sea (Millot 1990); (iii) the Rhône River which is the main fresh water source of the GoL. A general description of the hydrodynamics of the GoL is provided by Millot (1990). The existence of an anticyclonic circulation in the western part of the gulf following upwelling phenomena and an offshore drift of surface water has been first hypothesized in Millot (1979) and Millot (1982). Later, Estournel et al. (2003) showed an anticyclonic eddy located at the center of

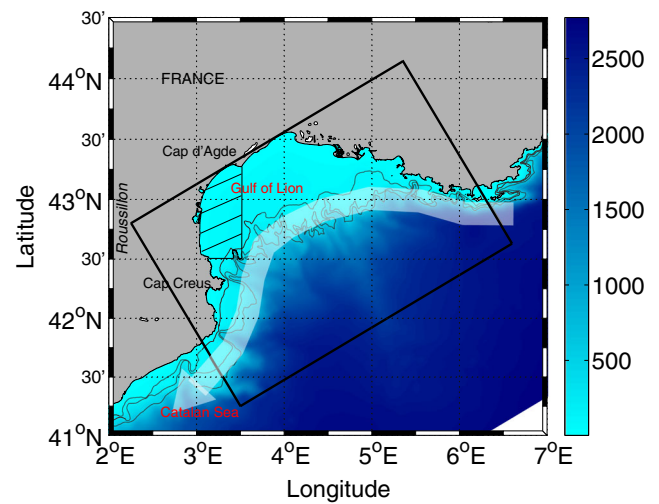


Fig. 1 Bathymetry of the Gulf of Lion. The *rectangle* represents the 1-km resolution model domain. *Shaded color* represents the bathymetry [m]. Isobaths at 100, 200, and 500 m are plotted with *thin lines*. The *white arrow* shows the mean position of the Northern Current (NC). The *hatched area* indicates the zone where the absolute value of potential energy anomaly ϕ is calculated

the GoL continental shelf or an anticyclonic circulation covering the western and center parts of the GoL, using both observations and model. On the eastern part of the GoL continental shelf, eddies are generated by the local wind (Allou et al. 2010; Schaeffer et al. 2011). (Sub)mesoscale processes are quite active also offshore the GoL, where sub-mesoscale coherent vortices can be formed in regions of deep convection (Bosse et al. 2016).

The GoL is particularly appropriate for studying coastal mesoscale dynamics and its role in regulating cross-shelf exchanges. Before the LATEX campaigns, two processes were recognized as main contributors to the exchanges between the GoL and offshore waters: dense shelf water cascading (Durrieu de Madron et al. 2012; Canals et al. 2006) and more shallow processes associated with the NC (Millot and Taupier-Letage 2005). Intrusions of the NC on the continental shelf of the GoL have been studied in the western (Millot and Wald 1980; Petrenko et al. 2008), central (Estournel et al. 2003; Petrenko 2003), and eastern parts (Petrenko et al. 2005; Barrier et al. 2016) of the GoL. On the eastern side, the flux of some of these intrusion events were estimated with *in situ* data, ranging between 0.37 Sv (Petrenko et al. 2013) and 0.5 Sv (Petrenko et al. 2005). By 2006, some (sub)mesoscale processes had been identified and studied on the eastern side of the GoL (Petrenko et al. 2005) and in its central region, especially linked to the Rhône river plume (Naudin et al. 1997; Broche et al. 1998). However, in the western part of the GoL, the focus had been mainly on dense water formation (Durrieu de Madron et al. 2005), while smaller scale processes had been relatively poorly investigated. The LATEX project aimed at

filling this gap, addressing -in its physics component- three main questions:

- What are the generation mechanisms and the general characteristics of (sub)mesoscale processes in the western GoL?
- How can field experiments be designed to investigate coastal (sub)mesoscale structures ?
- How much horizontal mixing and cross-shelf exchanges are associated with these processes?

After a brief introduction to the LATEX project (Section 2), this review will provide answers to these questions. Each question will be addressed in one specific section: dynamics in the western GoL (Section 3), *in situ* sampling strategies (Section 4), calculation of horizontal mixing and exchanges (Section 5). Finally, the Conclusion and Perspectives are drawn in Sections 6 and 7, respectively.

2 Data and methods

Numerical model simulations and *in situ* observations from a series of field experiments enabled us to answer the three main questions raised above.

2.1 Numerical modeling

The LATEX project included a numerical component whose initial objective, during the pilot phase, was to study the probability of occurrence of stable mesoscale structures in the GoL (Hu et al. 2009). Once this was positively achieved, the modeling component aimed at two main objectives: (1) to investigate the mechanism of formation and the characteristics of these structures and (2) to provide additional information to integrate/complement the analysis from *in situ* observations.

The model used in the project was Symphonie (Marsaleix et al. 2006; Marsaleix et al. 2008), a 3D primitive equation, free surface, sigma coordinate ocean model, based on the Boussinesq and hydrostatic approximations. Components of current, temperature, and salinity are computed on an Arakawa-C grid using a classic finite difference method. The vertical turbulence closure is achieved through a prognostic equation for the turbulent kinetic energy and a diagnostic equation for the mixing and dissipation length scales (Gaspar et al. 1990). As part of the pilot LATEX project in 2007, an optimized configuration of the Symphonie model was established for the Northwestern Mediterranean Sea (3 km resolution), with a nested high-resolution (1 km) model in the GoL (Hu et al. 2009). The high-resolution model domain is shown in Fig. 1.

Using this configuration, a realistic simulation was performed over 10 years, from 2001 to 2010. The initial and

open boundary conditions for the larger domain were provided by the Mediterranean Forecasting System (MFS, <http://eurogoos.eu/member-product/mediterranean-ocean-forecasting-system/>) general circulation model (Pinardi 2003) with a resolution of $1/8^\circ$. The atmospheric forcing was obtained from the 3-hr outputs of the meteorological model Aladin of Météo-France with a spatial resolution of $0.1^\circ \times 0.1^\circ$. The daily fresh water fluxes from the major rivers were taken into account. No data assimilation was included in the simulation. The readers are referred to Hu et al. (2009) and Hu et al. (2011a) for more details about the model settings.

The simulation was used to characterize the stable mesoscale processes in the western part of the GoL. The utility program WATERS (Doglioli et al. 2007) was used to objectively identify and follow coherent eddy structures. The method is based on wavelet analysis of horizontal slices of modeled relative vorticity. It detects the contour and the center of a coherent structure and monitors its characteristics over time and space. The numerical outputs also provided information on the larger scale dynamical context of the processes taking place before, during, and after the field cruises.

2.2 Satellite-derived products

Satellite data include SeaWiFs chlorophyll concentration (from NASA Goddard Space Flight Center) and a pseudo-SST (Sea Surface brilliance Temperature provided by Météo-France and corresponding to channel 4 of the AVHRR sensor: Advanced Very High Resolution Radiometer). These were used to identify, and follow in time, the signatures of the (sub)mesoscale processes in chlorophyll concentration and temperature. Surface geostrophic velocities produced by Ssalto/Duacs (Ssalto: ground Segment for multi-missions of altimetry, orbitography and precise location; Duacs: Developing use of altimetry for climate studies; $1/8^\circ$ resolution over the Mediterranean basin) and distributed by AVISO, with support from CNES (AVISO Archiving, Validation and Interpretation of Satellite Oceanographic data; CNES French National Center for Spatial Studies, <http://www.aviso.altimetry.fr/duacs/>) were used for Finite Size Lyapunov Exponent (FSLE) analysis. Detailed description of the processing and corrections of AVISO satellite altimetry can be found in the Ssalto/Duacs User Handbook (2010).

Along with Finite Time Lyapunov Exponents (FTLEs) (Haller and Yuan 2000), FSLEs (Aurell et al. 1997) have recently emerged as a powerful Lagrangian diagnostic for the investigation of the dispersion properties of a flow. Both methods measure the separation rate of the trajectories of close initial particles and can be applied for two complementary goals: quantifying dispersion processes. (Waugh and

Abraham 2008; Haza et al. 2010; Lumpkin and Elipot 2010; Schroeder et al. 2011), or mapping Lagrangian Coherent Structures (LCSs) (Haller and Yuan 2000; d'Ovidio et al. 2004; Olascoaga et al. 2006; Lehahn et al. 2007; Beron Vera et al. 2008; Haller 2011). Repulsive and attractive LCSs are associated with hyperbolic points of the flow and provide direct information on transport and mixing patterns (Mancho et al. 2008): particles spread while moving toward hyperbolic points along repelling LCSs, whereas they aggregate while moving away from hyperbolic points along attracting LCSs, which thus represent transport barriers (Lehahn et al. 2007; Haller 2011). The spatial organization of these structures has a large impact on the coastal environment, not only because they influence the dispersion of any tracer in the water, but also because, by separating dynamically distinct regions of the flow, they can define fluid dynamical niches which contribute to the structuring of marine ecosystems (d'Ovidio et al. 2010) and top predator distribution (Tew Kai et al. 2009; Cotté et al. 2011; De Monte et al. 2012). Generally, this altimetry based approach is less reliable in coastal regions, where the different ageostrophic dynamics induced by boundaries and nearshore forcings (Csanady 1982), insufficient sampling, presence of land mass and inaccuracy of geophysical corrections (Bouffard et al. 2008) represent critical limiting factors for altimetry. For this reason, during the campaign of September 2010 (see Section 2.3), daily maps of FSLEs were produced from real-time maps of absolute dynamic topography as a first guess of transport barriers and frontal systems, which were then precisely located by an adaptive strategy. The altimetry-derived FSLE maps, used in Nencioli et al. (2011) and in this current review paper, were re-processed after the campaign using the delayed-time maps of absolute topography. The near-real time and delayed-time products did not show large differences in the study area.

2.3 Field experiments

The LATEX project involved four cruises:

- Latex00, a preliminary three-day test cruise (June 9–11, 2007), (Petrenko 2007);
- Latex08, a one-week cruise to study an eddy (Sept. 1–6, 2008), (Petrenko 2008);
- Latex09, a one-week cruise dedicated to study another eddy (Aug. 25–30, 2009), (Petrenko 2009);
- Latex10, a tracer, multidisciplinary cruise conducted from two R/Vs (Sept. 1–24, 2010), (Petrenko 2010).

Note that, in the nomenclature for the cruises: LatexYY, YY indicates the year of the cruise for the second to the fourth cruise. The initial pilot cruise kept its original official name, Latex00, despite having taken place in 2007.

Latex08 and Latex09 These two LATEX field cruises focused on the detection and study of coastal mesoscale structures (Hu et al. 2011b; Kersalé et al. 2013). They took place on board the *R/V Téthys II*. A VMBB-150 KHz ship-based Acoustic Doppler Current Profiler (ADCP) was used to measure current velocities every 4 meters down to 247 m depth (see Petrenko et al. 2005 for details). At chosen stations, profiles were collected using a SeaBird SBE 19 conductivity-temperature-depth (CTD) sensor. During Latex08, since the sea state did not allow the use of the CTD, temperature profiles were obtained by using XBTs (eXpendableBathyThermographs). In addition, sea surface temperature, salinity, and fluorescence were measured continuously at the surface by the ship thermosalinograph SBE 21 and fluorometer. Wind was measured at 10 m above the surface. Technocean Surface Velocity Program (SVP) subsurface drifters, equipped with a 6 m long holey-sock drogue extending between 12 and 18 m, were deployed in the eddy to track the fluid motion at 15 m depth. Drifter positions were provided by the Argos system in quasi-real-time.

Latex00 and Latex10 These two LATEX field campaigns were dedicated to a tracer release experiment.

The first one, Latex00, was part of a pilot project which aimed to demonstrate the feasibility of our Lagrangian methodology and of a SF_6 tracer experiment in the GoL. To our knowledge, at the time of LATEX, only one SF_6 tracer experiment had taken place in a coastal environment (Wanninkhof et al. 1997). SF_6 is a gaseous electrical insulator with a very low solubility in seawater, which results in a background concentration in the seawater of about 0.3 fmol l^{-1} ($\text{fmol} = 10^{-15} \text{ mol}$). SF_6 can be detected at these low concentrations using the high sensitivity of gas chromatography with an electronic capture detector (Law et al. 1994). During Latex00, the background concentrations of SF_6 were measured in the surface mixed layer of the GoL. The values were around 1.35 fmol l^{-1} , which is the concentration of SF_6 expected for seawater in equilibrium with the atmosphere. Therefore, during the Latex10 cruise, it was possible to use a volume of 4 m^3 of seawater saturated with SF_6 to release a patch of $50 \text{ km}^2 \times 50 \text{ m}$, with SF_6 concentrations roughly 200 times higher than the background value.

The main goal of the last field experiment, Latex10, was to analyze the transport patterns and dispersion rates induced by a mesoscale structure within the Lagrangian reference frame associated with it. Therefore, the experiment was designed to combine the release of SF_6 with the deployment of an array of Lagrangian buoys. Latex10 involved the coordination of two R/Vs, one (the *R/V Le Suroît*) dedicated to the SF_6 experiment and the other one (the *R/V Téthys II*) dedicated to the survey of the underlying (sub)mesoscale processes. To successfully monitor such processes, the sampling strategy of the *R/V Téthys II* was

routinely optimized and adapted (hence “adaptive strategy”) in a Lagrangian framework based on the near real-time analysis of all the available *in situ*, remote or modeled data (see also Section 4). *In situ* measurements collected by the *R/V Téthys II* were similar to the ones during Latex09 (see above). In addition, turbulence profiles, down to 50 m, were acquired with a SCAMP (Self-Contained Autonomous Microstructure Profile). Lagrangian SVP subsurface drifters were released from both the *R/V Téthys II* and the *R/V Le Suroît*. Some were captured afterwards in order to be redeployed according to the near real-time analysis of LCSs (see Nencioli et al. 2011 for more details). The tracer release and mapping were performed from the *R/V Le Suroît*. The strategy was defined in coordination with the *R/V Téthys II* based on the Lagrangian navigation software (see Section 4.3). On the *R/V Le Suroît*, a VMBB-150 KHz hull-mounted ADCP provided current velocities every 8 m when depth was superior to 300 m or every 4 m in shallow waters. As on the *R/V Téthys II*, the *R/V Le Suroît* thermosalinograph/fluorometer measured surface temperature, salinity, and fluorescence along the ship transects. Wind was measured at 18 m above the surface. Numerous biogeochemical and biological measurements were also collected by the *R/V Le Suroît*, but their analysis is beyond the scope of this physics review paper. Up to three gliders were coordinated (L. Mortier and P. Testor, LOCEAN, Paris; L. Beguery, DT INSU, La Seyne sur Mer, France) to circulate in the zone at the time of the study. Their positions, and derived current velocities along their routes, were sent in near real-time to the two R/Vs to provide a global view of the general circulation around the study area. The analysis of the current, temperature, and salinity fields produced by the MFS was also sent to the *R/V Téthys II* to be taken into account in the adaptive strategy. The interested reader can refer to the two Latex10 cruise reports for additional details (available on www.mio.univ-amu.fr/LATEX;Publications section).

3 Dynamics in the western GoL

3.1 Numerical model results

The numerical simulations showed that mesoscale structures were common in the western part of the GoL during stratified conditions. Structures that last more than 15 days were qualified as “long-life” (Hu et al. 2011a). This limit of 15 days was chosen after several sensitivity tests. It represents a typical scale below which, in this coastal area and during stratified conditions, structures are considered submesoscale both temporally and spatially. All long-life features were anticyclonic baroclinic eddies. The results from the numerical simulation were then further investigated to better understand the generation processes and characteristics of these eddies.

The most common process of generation (Hu et al. 2011a) is due to a combined effect of wind forcing and topography, involving upwelling (south of Cape d’Agde) and Ekman transport southwestward (Fig. 2). These last two processes are generally due to strong northwest (NW) wind bursts, lasting more than 3 days. Once an eddy is created, strong stratification allows for a better transfer of wind-induced potential energy to eddy kinetic energy. However, additional strong wind bursts are also required to sustain the eddy in size and intensity. All details about the strength and persistence of the wind forcing can be found in Hu et al. (2011a). The level of stratification was estimated from the Symphonie numerical output by calculating the absolute value of potential energy anomaly, ϕ , throughout the water column of the eddy generation area (hatched area on Fig. 1). ϕ was shown to be a good indicator of the water column stability (Hu et al. 2011a; De Boer et al. 2008; Burchard and Burchard 2008). The more stratified the water column, the higher the value of ϕ . The reader can refer to Hu et al. (2011a) for more details on this calculation. Over the ten-year simulation (Fig. 3), the stratified conditions were classified into three major categories, according to the range of ϕ :

1. A weak stratification with a value of ϕ below 20 J m^{-3} , as during the winter-spring season;
2. An intermediate stratification with a value of ϕ around 60 J m^{-3} ; as during early May and late October for all years between 2001 and 2010, along with summers 2002 and 2004;
3. A strong stratification with a value of ϕ reaching 100 J m^{-3} , as during all summer seasons except in 2002 and 2004.

When stratification is not high enough, an eddy can be generated but it does not last longer than the time threshold of 15 days, and is classified as transient. The most stratified conditions are observed during the months of July to October (Fig. 3) and coincide with the occurrence of all the long-life eddies modeled in the GoL.

A second generation process has also been identified (Kersalé et al. 2013). This other process requires the presence of a $\mathcal{O}(100 \text{ km})$ anticyclonic circulation ($3^\circ - 4^\circ \text{ E}$ and $42^\circ - 43^\circ \text{ N}$) and a strong meandering of the NC (Fig. 4). The NC pushes the anticyclonic structure towards the coast, squeezing it so that it finally splits into two structures. The northern one, an anticyclonic baroclinic eddy similar to the wind-induced eddies previously described, remains in its area of formation over the continental shelf. The southern structure, on the other hand, does eventually migrate southward to the Catalan basin, contributing to the cross-shelf exchanges described in more detail in Section 5.2.

According to the daily numerical outputs, 11 long-life anticyclonic eddies have occurred during the ten-year period of the simulation (Fig. 5). They are present only during the

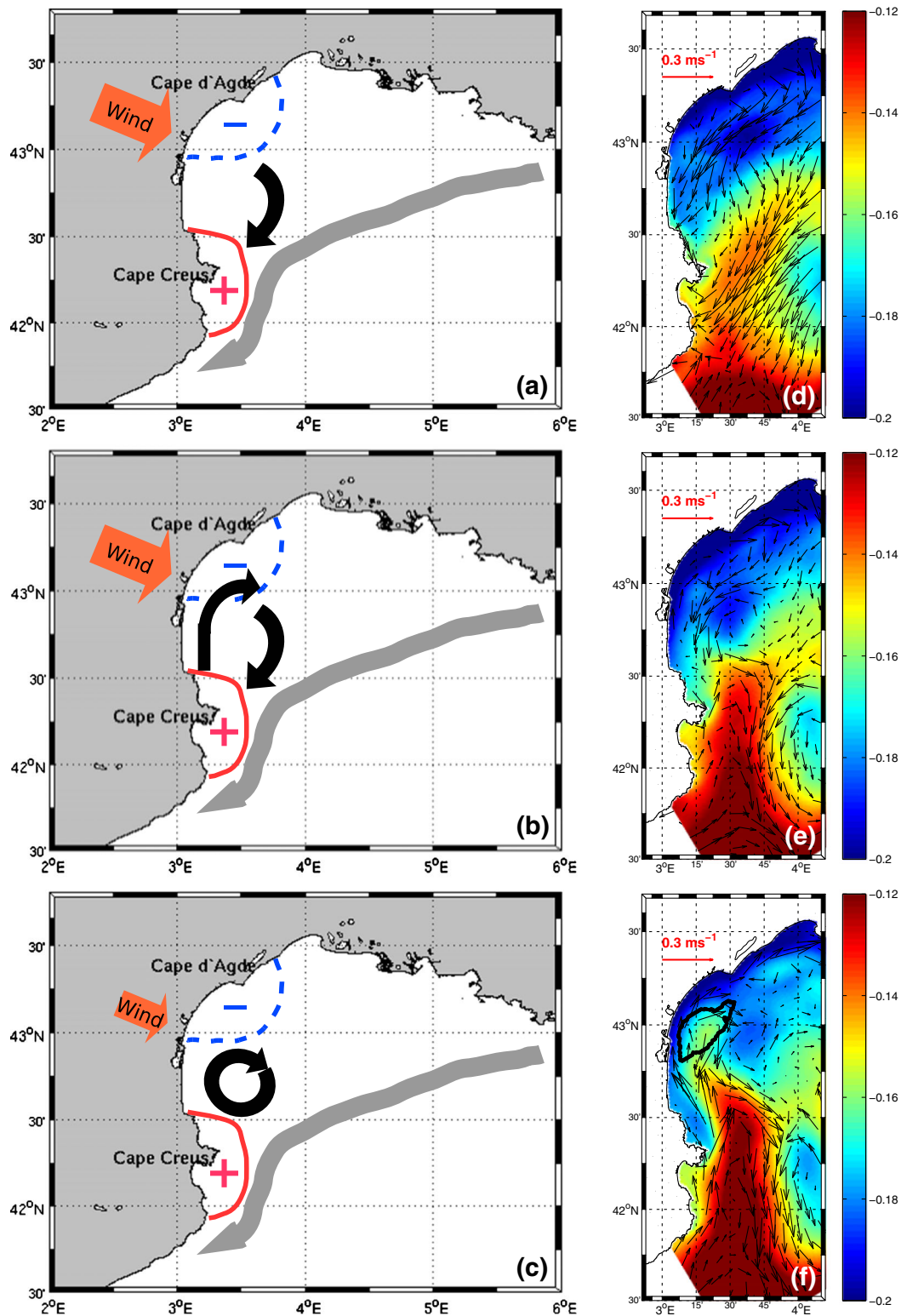


Fig. 2 Schematic generation of an anticyclonic eddy (from the 8-year numerical study of Hu et al. (2011b)). The three main phases of the eddy generation process are represented as follows: **a** upwelling and Ekman flow, **b** generation of a northward coastal jet, and **c** eddy generation. Eddy-related currents are represented by *black arrows*; upwelling area, corresponding to a negative Sea Level Anomaly (SLA), designated by the *blue dashes around the minus sign*; positive

SLA area around Cape Creus designated by the *red area around the positive sign*; wind represented by the *orange arrow*; the NC by the *grey arrow* along the continental shelf. As an example, corresponding modeled sea surface height and velocity field at 5 m depth on **d** July 02, 2005; **e** July 07, 2005; and **f** July 10, 2005. Black contour in **f** shows the eddy identification issued from the wavelet analysis

Fig. 3 Time series of 30-day moving averaged potential energy anomaly (Jm^{-3}) over the western part of the GoL for the upper 100 m depth for the years **a** 2001 to 2005 and **b** 2006 to 2010

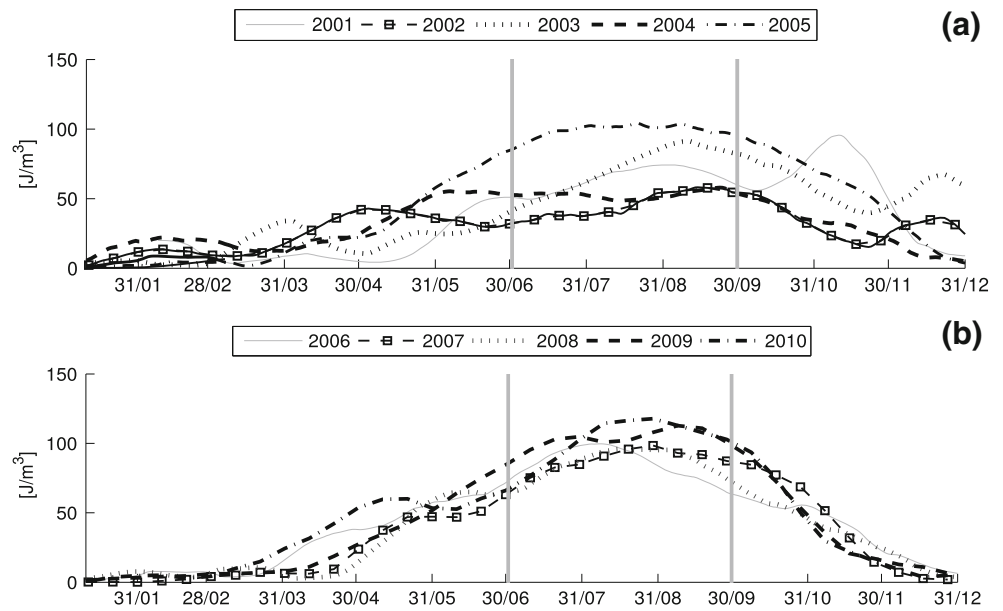


Fig. 4 Temporal sequence of formation of the eddy, sea surface height (m) and velocity field at 5 m depth (ms^{-1}) during the temporal sequence of formation of the eddy, in four steps: July 20, Aug. 8, Aug. 16, and Aug. 27, 2009 (adapted from Kersalé et al. (2013), with permission). Black contours in **c** and **d** show the eddies identification issued from the wavelet analysis

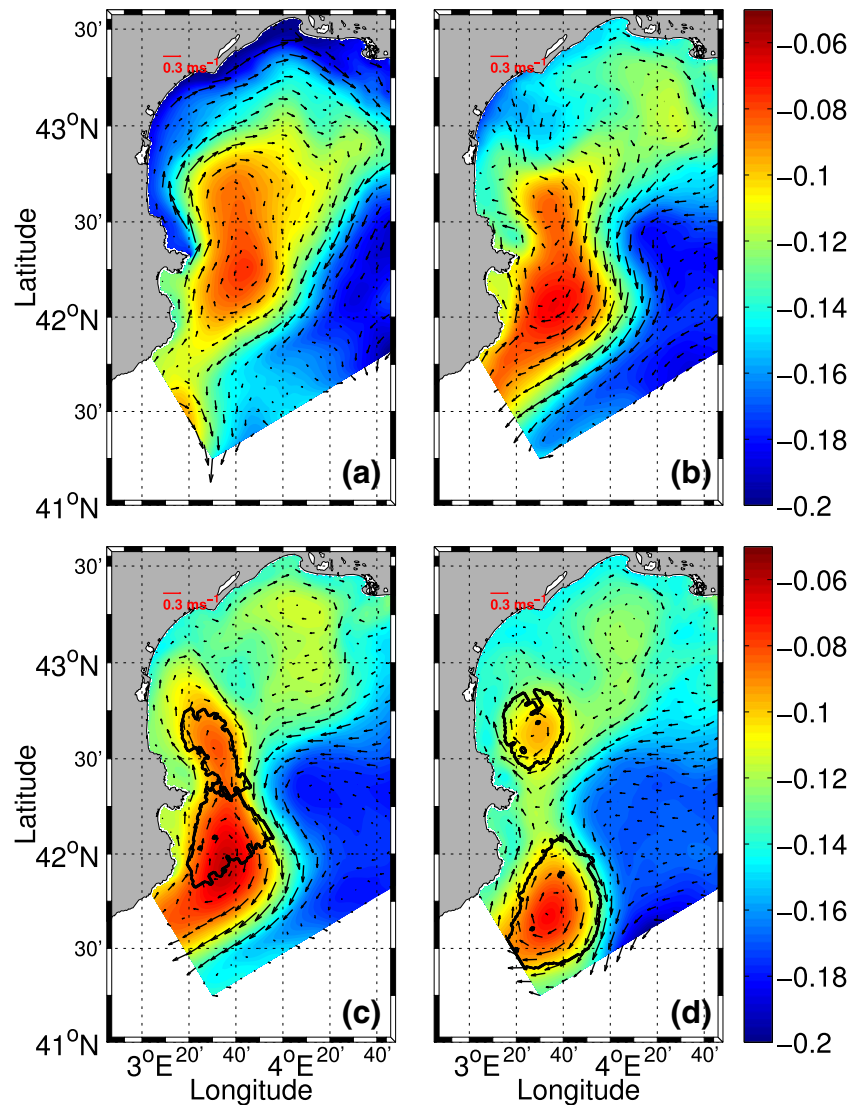
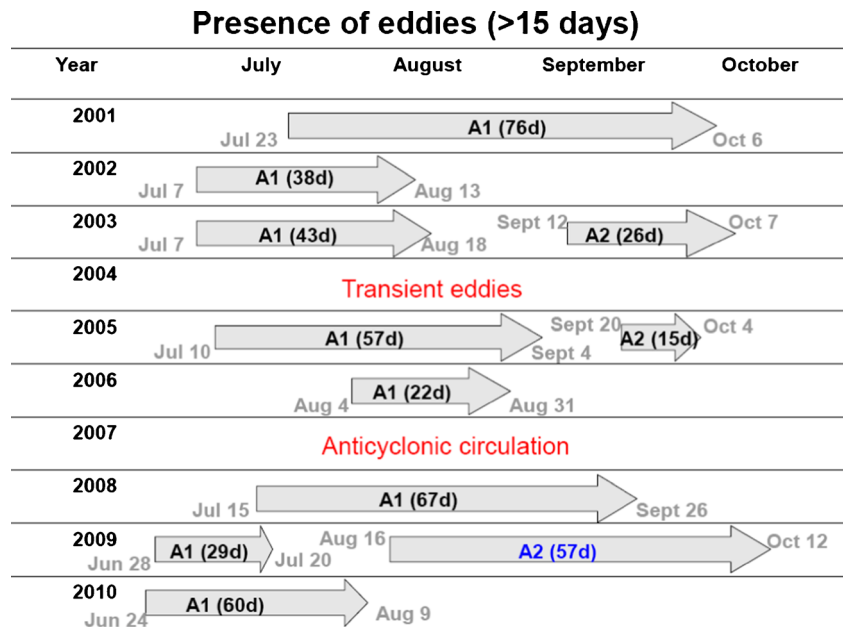


Fig. 5 Gantt table of the long-life modeled eddies from 2001 to 2010. The *grey arrows* indicate the duration of the first A1 or second A2 eddies, with the corresponding number of days in parenthesis. When this is written in *black*, the eddy has been generated with the first generation process (Hu et al. 2011b). When in *blue*, it has been generated by the second generation process (Kersalé et al. 2013). The dates of birth and death of each eddy are also indicated



stratified period from July to October of a given year. The mean duration of these eddies is 44.5 days (with a standard deviation of 20 days), which is long in a rapidly-varying coastal environment such as the GoL. Among these 11 vortices, only one was formed by the second process (Kersalé et al. 2013), while the other 10 are explained by the first generation process (Hu et al. 2011a). Throughout the years, the eddies occurred as follows:

- Years without eddies (2004, 2007),
- Years with 1 eddy (2001, 2002, 2006, 2008, and 2010),
- Years with 2 eddies (2003, 2005, and 2009).

Hereafter, vortices are called LatexA(i).YY, with an A to specify that the eddy is anticyclonic, and potentially an i to indicate that this is the i-th eddy of year YY for the years with more than one eddy.

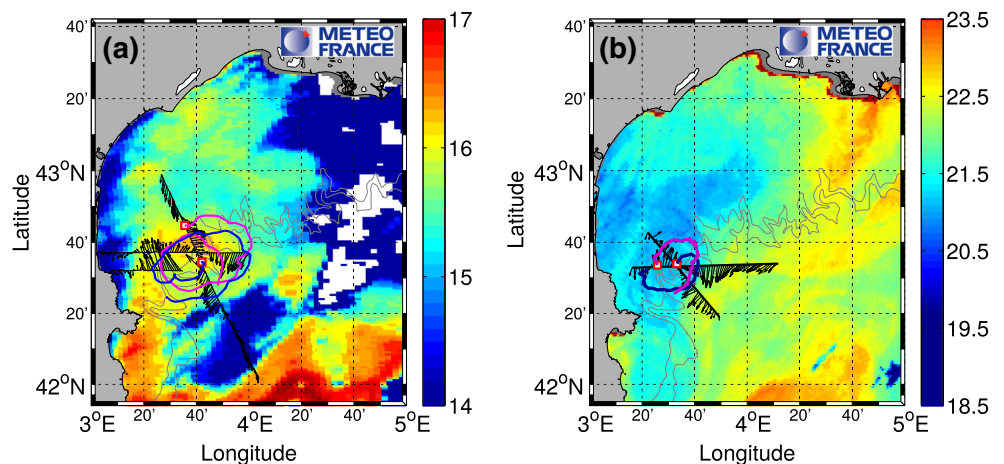
The years 2004 and 2007 stand out as unusual because they had no long-life eddy. In 2004, transients eddies

appeared but no long-life eddy ever occurred despite successive strong NW wind events, probably due to the weakness of the summer stratification (Fig. 3). In 2007, since the stratification was strong and the wind forcing was particularly intense, the mesoscale eddy increased in scale and became an anticyclonic circulation larger than the study area (see Fig. 4 of Hu et al. 2011a). Furthermore, a third year was also found to be anomalous. In 2002, a long-life eddy existed despite an intermediate level of stratification (Fig. 3). This occurred because, as in 2007, the wind forcing was particularly strong, persistent, and frequent.

3.2 In situ observations

Numerical model results have been complemented with *in situ* observations from the Latex08 and Latex09 campaigns to study the characteristics of these structures (Fig. 6). Both

Fig. 6 Eddies studied **a** during Latex08 and **b** during Latex09. ADCP transects, with horizontal currents at 15 m depth in *black*. SVP drifter trajectories shown in *blue* and *purple* during **a** 6 days and **b** 3 days following their release at the location indicated with a *red square*. Pseudo-SST images on **a** Sept. 02, 2008 and **b** Aug. 28, 2009



datasets showed that these eddies are baroclinic, mainly confined within the mixed layer depth (about 30 m), and generally elliptical (Hu et al. 2011a; Kersalé et al. 2013). They have a diameter of about 20 km and tangential speed of the order of $0.3\text{--}0.4\text{ m s}^{-1}$ on the outer edge so that a full loop around the eddy takes ~ 3 days. When possible, the characteristics of the modeled eddies were compared with those measured and showed very good agreement (Hu et al. 2011a; Kersalé et al. 2013). For instance, the characteristics of the second long-life anticyclonic eddy of 2009, hereafter LatexA2.09, were compared. The center of the eddy was estimated at $3^{\circ}26'$ E – $42^{\circ}36'$ N in the model and at $3^{\circ}34'$ E – $42^{\circ}33'$ N from *in situ* velocity cross-sections of the eddy (see Section 4.1). The radial distribution of tangential velocities (see Fig. 3 of Kersalé et al. 2013 and accompanying text) was also used to estimate the region of the eddy in solid-body rotation, and hence its horizontal diameter. Tangential velocities linearly increased to average maximum values V_{\max} of $\sim 0.35\text{ m s}^{-1}$, at radial distances R_{\max} between 9 and 15 km. Thus, the *in situ* estimate of eddy dimensions is very close to that from the model (mean radius of 14.3 km based on the WATERS wavelet analysis described in Section 2.1). Analogously, the eddy vertical extents from model and observations were also very close, being 37 and 35 m, respectively. The local Rossby number R_o and the Rossby radius of deformation R_d were also estimated at 0.26 and 5.9 km, respectively. Since $R_{\max} > R_d$, this eddy was classified as a mesoscale structure. Nonetheless, the local Rossby number was not small, so its dynamics could not be approximated by quasi-geostrophic theory.

Coastal dynamics was quite different for the Latex10 campaign in September 2010, during which no anticyclonic structure was present. AVHRR pseudo-SST imagery showed that the circulation in the western part of the GoL was characterized by the development of a strong thermal front (Fig. 7c). The combined analysis of ship-based and Lagrangian observations revealed that the front was associated with an intense flow 10 km wide and roughly parallel to the coast, through which waters from the continental shelf left the GoL towards the Catalan Basin (Nencioli et al. 2011). The front was formed due to the convergence, and the resulting stirring, of warmer open Northwestern Mediterranean waters, with colder waters on the continental shelf (respectively, O and C waters in Nencioli et al. (2013, 2016)). Analysis of wind data and drifter trajectories indicated that the movement of the former was mainly driven by the NC dynamics along the continental slope, whereas the latter were advected southward out of the GoL due to Ekman flow following strong NW wind events. Therefore, the front formation was mainly driven by the stirring induced by the interaction between wind-induced and large-scale circulation (Nencioli et al. 2016).

Analysis of temperature, salinity, and density data from cross-front transects showed that the front was mostly density-compensated (Nencioli et al. 2013). Temperature (salinity) gradients could reach up to 2°C (0.4 psu) over less than 4 km across the front. The distribution of the vorticity Rossby number across the front showed predominant values smaller than $\mathcal{O}(1)$, with occasional maxima around $\mathcal{O}(1)$ (Nencioli et al. 2016, SI, Fig. 6). This indicated that the Latex10 front was mainly associated with geostrophic (i.e., mesoscale) dynamics. Therefore, although a surface intensified geostrophic flow and stronger vertical velocities may have occasionally occurred where the horizontal density gradient and relative vertical vorticity were large, the role of the local frontal dynamics was not explored. The implicit assumption is that horizontal advection by the geostrophic and Ekman flows that induced the formation of the front had stronger impact on the front's dynamics and temporal evolution than secondary ageostrophic circulation (Nencioli et al. 2013, 2016).

4 Design of field experiments to investigate coastal (sub)mesoscale structures

A powerful approach to quantify complex and ephemeral physical coastal processes is to perform the study in a Lagrangian reference frame with an adaptive strategy. This allows for the deconvolution of advection versus dispersion processes. At the time of the submission of the LATEX project to funding agencies, Lagrangian strategies were not as commonly used as now. Together with Griffa et al. (2007), LATEX was a pioneer study in adopting this type of approach. The main three examples of adaptive Lagrangian sampling strategy used during LATEX are presented in the next subsections.

4.1 Eddy *in situ* tracking (Latex08 and Latex09 - R/V *Téthys II*)

During Latex08 and Latex09, a methodology to identify, follow and *in situ* sample an eddy, was developed, tested and improved. Before the cruise, analysis of pseudo-SST and ocean color satellite imagery was used to identify the presence of mesoscale eddies. If an eddy was detected, its center and potential translation speed were estimated with these data. This information was compared to and integrated with the results from the numerical simulations described in Section 2.1. The results were used to define the position and orientation of the first radial section across the eddy center for the collection of *in situ* ADCP and CTD (or XBT in case of bad sea conditions) observations. The ADCP measurements collected by the ship hull-mounted ADCP were then used to identify the position of the eddy center after

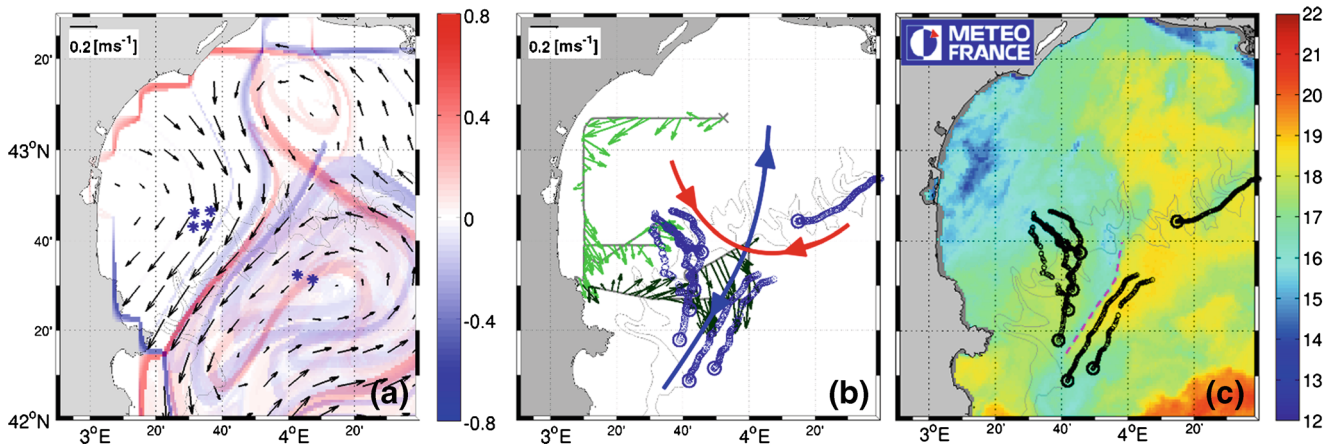


Fig. 7 **a** Lagrangian coherent structures, FSLE in (d^{-1}) derived from AVISO geostrophic velocities on Sept. 14, 2010 and release position of the Lyap01 cluster of Lagrangian drifters. In *blue* are the attracting LCS (backward FSLE) and in *red* the repelling ones (forward FSLE). **b** ADCP currents, 3-day drifter trajectories and position of

the Lagrangian coherent structures reconstructed from *in situ* measurements. **c** Image of pseudo-SST for Sept. 14, 2010 and 3-day drifter trajectories. The position of the front focus of the Latex10 field experiment is marked by the *magenta dashed line*. (adapted from Nencioli et al. (2011, 2016) with permission)

each ship transect based on the algorithm developed by Nencioli et al. (2008). In the case of Latex08, this was done post cruise. However, for Latex09, the data processing chain was optimized and the work was done on board in near real-time. This way, the precision of the center position was greatly improved compared to that estimated qualitatively from satellite imagery. The sampling strategy of the rest of the campaign was adapted with respect to each new calculated eddy center position, with the deployment of SVP drifters at the center or the edge of the eddy and multiple transects crossing the center either orthogonally or in a “butterfly” trajectory (Fig. 6 and refer to Hu et al. (2011b) and Kersalé et al. (2013) for details).

4.2 Direct LCS iterative sampling (Latex10 - *R/V Téthys II*)

During Latex10, in the absence of a marked mesoscale structure, instead of the planned tracking and tracer injection of an eddy, the strategy was adapted to a (sub)mesoscale process study. The complexity of features visible from satellite chlorophyll-*a* and pseudo-SST maps, model circulation outputs and glider data rendered this task particularly challenging. The process study included the direct real-time detection of LCSs. This was tested with a novel, iterative, *in situ* sampling strategy (Nencioli et al. 2011) which combined satellite altimetry data, ship-based ADCP measurements, and iterative Lagrangian drifter releases (Fig. 7). Three arrays of drifters were released at intervals of a few days to obtain *in situ* estimates of the structures. The dispersion pattern of the first drifter array on Sept. 12 confirmed the presence of the along-shelf LCSs associated with the NC identified from AVISO velocities (Fig. 7a). The deployment position and the spatial configuration of the second

and third array were chosen on the basis of the outcome of the previous launches. *In situ* repelling (red) and attracting (blue) LCSs identified and tracked the migration of an hyperbolic point for a period of 12 days, indicating that Lagrangian diagnostics such as FTLE and FSLE can be successfully identified even in the complex and variable flows typical of coastal regions (Nencioli et al. 2011). Nevertheless, *in situ*-based LCSs (also confirmed by ADCP observations) showed an opposite circulation compared to the AVISO field over the continental shelf, confirming the limitation of traditional altimetry for reliable transport analysis in those regions (Nencioli et al. 2011). To develop methods to mitigate such altimetry limitations in coastal environment, LATEX float trajectories were used to test the use of region-specific optimal interpolation methods to generate maps of satellite-derived geostrophic current anomalies, ultimately providing better absolute geostrophic currents, once added to different mean circulation fields (Bouffard et al. 2014). Otherwise, during the cruise, the identification of the LCSs contributed to accurately identifying the location of the thermal front described in Section 3 and tracking its evolution, particularly when satellite imagery of pseudo-SST and ocean color was not available due to cloud cover. This provided a decisive contribution for (i) optimizing the sampling strategy for the collection of cross-front sections (Section 5.1), and (ii) tracking the movement of water masses for the quantification of the cross-shelf fluxes associated with the front (Section 5.2).

4.3 Tracer release (Latex00 - *R/V Téthys II*, and Latex10 - *R/V Le Suroît*)

One of the goals of the Latex10 field experiment was to mark a dynamical mesoscale feature by releasing a passive

tracer together with an array of Lagrangian buoys. The goal was to release the tracer in an initial patch as homogeneous as possible in the horizontal, and to study its turbulent mixing and dispersion while minimizing the contribution due to the advection. For that, it was necessary to continuously adjust the vessel route in order to remain as closely as possible in the Lagrangian reference frame moving with the investigated mesoscale structure. To accomplish this task, two of the four LATEX field campaigns were dedicated to the development of such a methodology. The first campaign, Latex00, aimed at demonstrating its feasibility; the last one, Latex10, performed a final test followed by the actual tracer experiment.

To perform the initial tracer release and subsequent mappings in a Lagrangian reference frame, the movement of the targeted water mass was tracked using a reference buoy as a proxy. Our approach consisted in solving a classical ballistic problem to obtain, in real-time and in a moving water mass, the direction and distance to the next turn point of a chosen geometric route (details in Doglioli et al. 2013). Results from the two field experiments showed that accuracy and frequency of acquisition of both vessel and buoy positions are key aspects for the successful implementation of this methodology.

The observational experience and analytical tools developed within LATEX led to a successful Lagrangian tracer release during the Latex10 experiment. The area for the tracer dispersion experiment was selected combining the numerical model results with those from the near real-time analysis of FSLEs computed from satellite-altimetry derived currents (Nencioli et al. 2011). The tracer was released in a patch of dimensions roughly $25 \text{ km}^2 \times 25 \text{ m}$, smaller than initially planned. After the release, the horizontal evolution of the tracer patch was monitored for 7 days during a series of four successive horizontal mappings done at 7 m depth, the depth of the tracer release (Kersalé et al. 2015).

The software developed for the Lagrangian tracer experiment is included in the LATEXtools software suite (see Section 8). Our methodology presents some important technological improvements with respect to previous tracer studies related to both the positioning of the central buoy and the communication system with it. The software is also equipped with a series of graphical and user-friendly accessories.

5 Horizontal mixing and cross-shelf exchanges

The tracer experiment from the *R/V Le Suroît* during Latex10 allowed a first estimate of lateral diffusivity at (sub)mesoscale (Kersalé et al. 2015). A second estimate was obtained by combining the strain rate from the drifter

release, with the temperature and salinity gradients from thermosalinograph observations collected aboard the *R/V Téthys II* (Nencioli et al. 2013). Finally, the combined analysis of *in situ* measurements and numerical modeling results provided a quantification of surface cross-shelf fluxes in the western GoL, the ultimate goal of the LATEX project.

5.1 Lateral diffusivities from tracer release and cross-front transects

The dispersion of the patch of the passive tracer SF_6 , released in the adaptive Lagrangian framework described in Section 4.3, was used to obtain a first estimate of the lateral diffusivity in the coastal waters of the western part of the GoL. After having quantified the atmospheric loss of SF_6 , the temporal evolution of the patch was fit with a diffusion-strain model to obtain estimates of the strain rate $\gamma = 2.5 \cdot 10^{-6} \text{ s}^{-1}$ and of the lateral diffusivity coefficient $K_h = 23.2 \text{ m}^2 \text{ s}^{-1}$ (Fig. 8, top panel). To test the robustness of this estimate, a steady state model was also applied, showing K_h values similar to the diffusion-strain model after a period of adjustment between 2 and 4.5 days. This implied that, after such period, the computation of K_h became independent from the further straining of the patch. The presence of the thermal front southeast of the initial patch clearly affected the dynamics within the region and thus the temporal evolution of the patch (see Kersalé et al. 2015 for additional details). Nonetheless, the results were consistent with previous studies in the open ocean (refer to the end of the section for more details) and demonstrated the success and feasibility of these methods also under small-scale, rapidly-evolving dynamics typical of coastal environments. However, one should note that this type of approach is still a challenge. Among the difficulties encountered, some worth mentioning include issues related to fitting a Gaussian dispersion model to a patch which, under the stretching induced by the front, does not exhibit a Gaussian shape; technical limitations, making it difficult to sample the whole fast-dispersing patch, due both to vessel speed and SF_6 analysis time, affecting the sampling frequency. One of the objectives of the tracer experiment was also to determine the vertical diffusivity K_z , and to compare it with the values derived from turbulence profiles acquired with the SCAMP. However, lack of resolution in the vertical sampling of the tracer made the imprecision of the method too large to obtain reliable estimates. Nonetheless, turbulence profiles, acquired with the SCAMP, have been used in a numerical study investigating the impact of turbulence closure schemes and boundary conditions on the evaluation of K_z and energy dissipation rate (Costa et al. 2016).

A second estimate of *in situ* lateral diffusivity coefficients at the (sub)mesoscale was based on an analogous

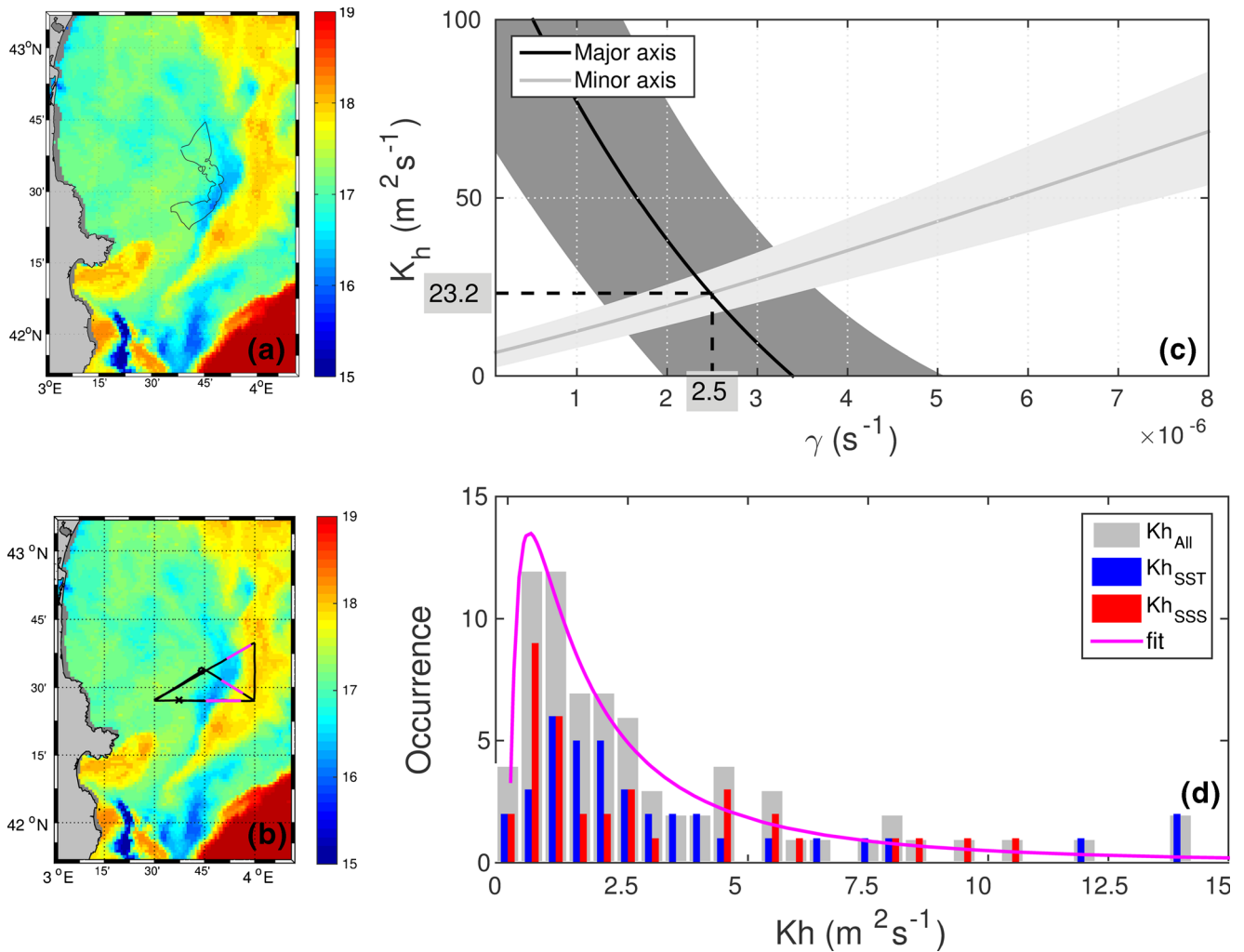


Fig. 8 Spatial scales and diffusivity coefficients. **a** Pseudo-SST map on Sept. 15, 2010 with the contour of the 3rd SF_6 mapping. **b** Pseudo-SST map with examples of cross-front transects, in magenta. **c** The point of intersection of the two curves (major and minor axes, see Kersalé et al. (2015) for details) indicates the best estimates of γ (s⁻¹) and K_h (m² s⁻¹). The shaded areas represent the uncertainties. **d**

Frequency histogram of the horizontal eddy diffusivity coefficients derived by Nencioli et al. (2013). In blue is the distribution of the K_h estimated from the SST profiles only; in red the distribution of the K_h from the SSS profiles only; and in grey the total distribution of the two combined together. In magenta is the fitted log-normal distribution

hypothesis of balance between mesoscale straining and small scale mixing adopted for passive tracer experiments. However, instead of using the shape of the tracer patch, the analysis was based this time on the width of the thermal-haline front (Nencioli et al. 2013). The assumption at the base of this second approach is that, once a near steady-state is reached, the shape of the front will result from the balance between its strain-induced steepening and its diffusion-induced relaxation. Such an approach has already been applied by Flament et al. (1985), who quantified eddy diffusivity by combining the cross-front width derived from temperature variations observed along a single ship-based cross-front section, with an approximate estimate of the cross-front convergence rate derived from successive satellite imagery of surface temperature. During Latex10,

a series of front widths were obtained, instead, by fitting multiple high-resolution temperature and salinity cross-front sections with an analytical model for the cross-front profile at the equilibrium. The front widths were then combined to the local strain rate estimates derived from the dispersion of two arrays of Lagrangian drifters to retrieve horizontal eddy diffusivities (see Nencioli 2013 for details on the equations). Latex10 adaptive sampling allowed the collection of 19 cross-front transects within a span of 9 days, from which a total of 76 estimates of lateral diffusivity K_h (19 SST transects, 19 SSS transects and two estimates of strain rate) were computed. Their distribution is log-normal with a broad peak at values below 2.5 m² s⁻¹, and a relatively long tail of episodic occurrences at values above 7.5 m² s⁻¹ (Fig. 8, bottom panel). The distribution ranged

from a lowest value of $0.06 \text{ m}^2 \text{ s}^{-1}$ to a maximum value of $46.67 \text{ m}^2 \text{ s}^{-1}$, with 70% of the values between 0.4 and $5 \text{ m}^2 \text{ s}^{-1}$. The mean K_h computed using all estimates available was $3.98 \text{ m}^2 \text{ s}^{-1}$, with a standard deviation of $7.26 \text{ m}^2 \text{ s}^{-1}$. Further details on K_h statistics, including the impact of higher but less frequent estimates, can be found in Nencioli et al. (2013). Despite some expected differences, the distribution of K_h estimated from the SST profiles was characterized by a similar shape as the one from the SSS profiles (Fig. 8, bottom panel). Moreover, it is noteworthy that, although being characterized by different ranges, SST and SSS gradients from the same section returned similar estimates of K_h . This was an important feature since it showed that the estimates of K_h using this approach were primarily controlled by the front width and were, at the same time, relatively independent from the magnitude of the tracer variation across the front.

The mean values of K_h obtained with the two methods corresponded, respectively, to spatial scales of the order of (i) the width of the patch (10 km) or (ii) the cross-front distance (here below 5 km). As mentioned in the introduction, at scales on the order of 10 km, lateral diffusivities had been found of the order of $10 \text{ m}^2 \text{ s}^{-1}$ (Ledwell and Watson 1991; Holtermann et al. 2012). These results are also in agreement with the estimates from the LatMix project in summer 2011, a year after Latex10. LatMix used different tracers (rhodamine and fluorescein) and mapping techniques (lidar) than LATEX. Isopycnal diffusivities were also calculated from drifter trajectories. The values obtained were of the order of $1 \text{ m}^2 \text{ s}^{-1}$ at scales on the order of 1–5 km (Shcherbina et al. 2015).

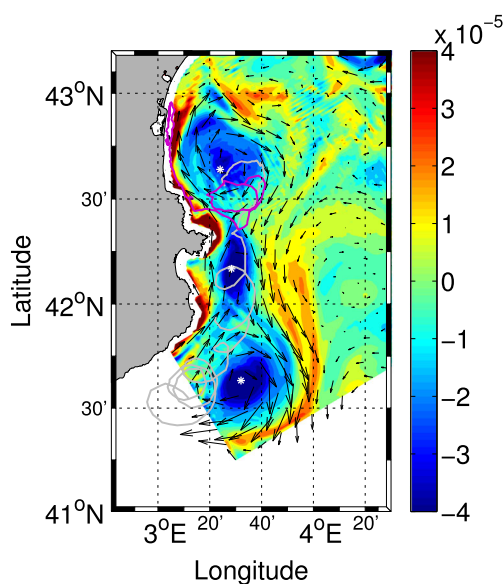


Fig. 9 Transient structure detaching from LatexA2_09. Modeled relative vorticity [s^{-1}], velocity field at 20 m depth on Sept. 3, 2009 (arrows) and drifter trajectories (grey and purple) from Aug. 26 to Sept. 11, 2009. The white stars represent each structure center

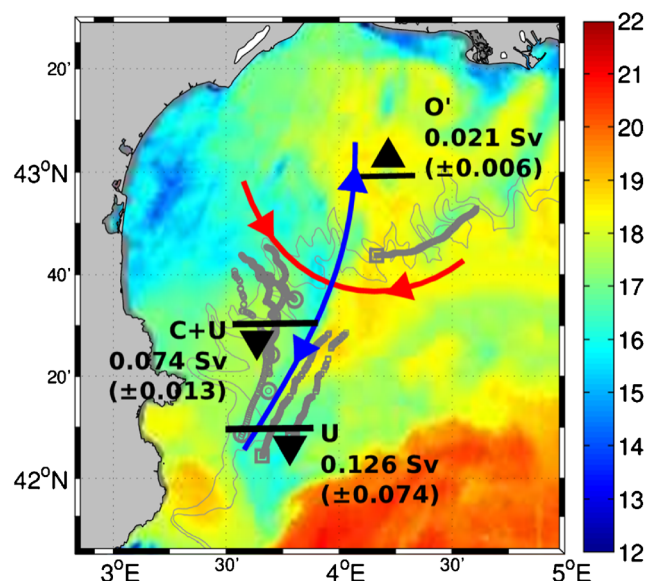


Fig. 10 Schematics of the average cross-shelf fluxes associated with the front from Latex10, superimposed on pseudo-SST, buoy trajectories (grey) and *in situ* LCSs (red and blue). Locations of outflow and inflow of the U (upwelled), C (coastal), and O' (modified open, see Nencioli et al. (2016) for details) waters are indicated relative to the Lyap01 LCS, as no cloud-free pseudo-SST images are available afterwards. (adapted from Nencioli et al. (2016) with permission)

5.2 Surface cross-shelf fluxes

During the LATEX project, two main dynamical situations were observed in the western part of the GoL:

1. The presence of an anticyclonic eddy, during which exchanges were investigated from a numerical model, backed-up by Latex09 observations;
2. The case of a frontal structure when no eddy was present; the exchanges were quantified from Latex10 observations.

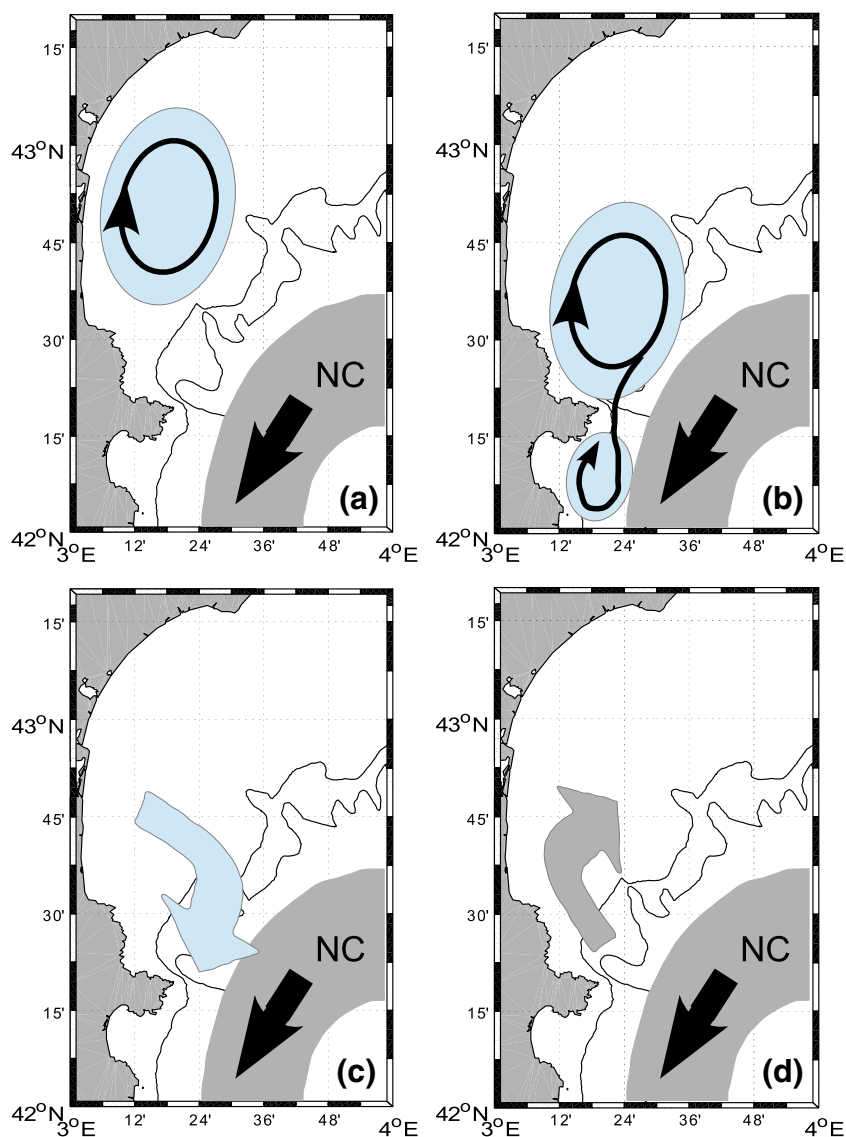
When a mesoscale structure is present in the western part of the GoL, it can lose a portion of itself by a peeling mechanism either linked to the topography (Nof 1999) or to the large-scale forcing (for example, squeezing by the NC such as in Kersalé et al. (2013), previously described in Section 3). These detached bits are generally transient structures, that can move relatively quickly out of the Gulf, contributing to the cross-shelf exchanges. In 2009, two Lagrangian floats, deployed in the LatexA2_09 eddy, rotated in it for, respectively, two and four and a half days (Fig. 9). The float that had stayed the longest in the eddy was then caught in the coastal northward jet. The other one left the eddy and moved southward performing anticyclonic rotations. These, although in the clockwise direction, were not due to inertial oscillations, since their period was about 39 h (while the near-inertial oscillations (NIO) have a period

of 17.5 h). The numerical simulations provided the necessary information to explain such drifter trajectory. Figure 9 shows the drifters trajectories superposed to modeled relative vorticity, suggesting that the southward moving drifter joined another eddy present in the Catalan basin. The position of the Catalan eddy is located in the model further east than suggested by the float rotations. Despite the use of hybrid sigma coordinates, the strong bathymetry gradients are probably responsible for this shift in modeled circulation features. Nevertheless, the numerical simulations confirmed the mass exchanges modulated by eddy activity between the GoL and the Catalan shelf. The mass of the transient structure represented a third of the initial LatexA2_09 eddy mass. The latter lost $\sim 40\%$ of its mass during the separation. The mass (or volume) contribution to the Catalan eddy could not be assessed, the latter being cut by the model boundary. The volume of the transient structure is estimated to 12.1 ± 0.1

km^3 . This flux leaving the GoL could occur several times during the life of an eddy.

When no mesoscale eddies are present, the outer edge of the western GoL is characterized by the thermal front observed during Latex10 (see Section 3). The analysis integrated the observations from multiple platforms in order to (i) identify the different water masses, their origins and track their movements; (ii) remove the signal associated with NIO from instantaneous ADCP velocities; and hence (iii) calculate accurate cross-shelf exchanges within the upper mixed layer associated with the front (Nencioli et al. 2016). Water masses were identified and tracked from successive satellite imagery and Lagrangian observations (see Section 2.3). The reconstructed *in situ* LCSs also provided a reference frame to quantify cross-shelf exchanges. Since the flow associated with the front was approximately non-divergent, the transport of a given water volume along the LCS tangent

Fig. 11 Schematic of four main circulation patterns in the western GoL. **a** Water eddy retention. **b** Transient feature leaking from eddy. **c** Cross-shelf flux exiting the GoL. **d** Coastal jet entering the GoL. Blue (grey) areas indicate the preferential zones of baroclinic (barotropic) circulation features



was conserved for different sections across the structures. Therefore, sections across the LCSs were used to compute cross-shelf exchanges even if not collected along the GoL boundary (i.e., the continental slope). Finally, Lagrangian drifter trajectories were also used to quantify NIO. Strong NIO can have important impacts on current strengths and fluxes in the region (Millot and Crépon 1981; Petrenko et al. 2005; Petrenko et al. 2008). Most of the Latex10 drifter trajectories exhibited several clockwise loops with period around ~ 17.5 h, indicating the presence of NIO. The time-series of their zonal and meridional components evidenced large oscillations superimposed to a slowly varying mean. As expected, the two components were out of phase by 90° , with positive meridional components preceding positive zonal ones. Following Haza et al. (2008), the mean velocity components were retrieved by applying a moving average based on a Gaussian window with a full width at half maximum (FWHM) of 17.5 h. The NIO components were then computed as the residuals, i.e., the difference between original and averaged values. These NIO components were removed from the instantaneous ADCP observations from the cross-front sections used to compute the cross-shelf exchanges. Limits of integration along each section were defined based on thermosalinograph observations which were used to identify the boundaries between the various outflowing and inflowing water masses.

The results indicated an average outflow of 0.074 ± 0.012 Sv and an inflow of 0.021 ± 0.006 Sv (Fig. 10). Integrated over the two-week lifetime of the front, such outflow would induce a total export of $\sim 90 \pm 14$ km³ of water. Thus, three to four of such events would be sufficient to completely renew the surface waters of the GoL. The total water import amounted to only $\sim 25 \pm 7$ km³, less than a third of the outflow, hence suggesting larger inflows at depth or in the eastern part of the gulf to maintain the GoL volume balance. These *in situ* estimates represent a key term of comparison for the further development of numerical model- and satellite-based studies of cross-shelf exchanges associated with this type of processes. These cross-shelf exchanges can have impacts on biogeochemistry and ecology, as they can regulate the fluxes of carbon (Bauer and Druffel 1998; Gattuso et al. 1998) and nutrients (Grantham et al. 2004), as well as the dispersion of fish-larvae (Roughan et al. 2006) and pollutants (Gustafsson et al. 1998).

6 Conclusion

The results of the physics component of the LATEX project have addressed the three main questions raised in Section 1.

- 1) Mesoscale dynamics in the western GoL includes coastal mesoscale eddies or strong fronts. The eddies are elliptic, baroclinic and anticyclonic. They are generated either by the combined effect of strong wind and stratification or by boundary current meanders (Hu et al. 2009; Hu et al. 2011a, b; Kersalé 2013). The observed strong thermal (and saline) front was density-compensated (Nencioli et al. 2013). The front generation was mainly driven by the stirring induced by the interaction between wind-forced and large-scale circulation.
- 2) Field experiments were designed to investigate coastal (sub)mesoscale structures. Throughout a series of successive oceanographic cruises, LATEX developed and optimized a methodology for an adaptive Lagrangian sampling. Such adaptive approach was successfully applied to detect coastal eddies (Hu et al. 2011b; Kersalé et al. 2013), to identify Lagrangian Coherent Structures (Nencioli et al. 2011), and used for the initial release of a passive tracer as homogeneously as possible in a Lagrangian framework (Doglioli et al. 2013).
- 3) Horizontal mixing and cross-shelf exchanges were quantified. Lateral diffusivity coefficients, calculated using different approaches, are in the range classically encountered for their associated scales (Kersalé et al. 2015; Nencioli et al. 2013). To calculate K_h , the project included both a more traditional passive tracer experiment, as well as a novel technique based on the combined analysis of strain rate and thermohaline gradients. The strain rate was obtained from the analysis of the Lyapunov exponents derived from the Lagrangian floats (Nencioli et al. 2013). Cross-shelf exchanges are strongly influenced by the dynamical conditions at the shelf edge. In the western GoL, these can be characterized by the presence of either mesoscale eddies or strong thermohaline fronts. Eddies can trap waters in their core (Hu et al. 2011a) but can also get eroded by the slope current, losing non negligible percentage of their mass (Kersalé et al. 2013) all the way to potentially disappearing in the process. Fronts can act like corridors favoring strong cross-shelf inter-regional exchanges (Nencioli et al. 2016).

This paper has summarized the (sub)mesoscale dynamics studied during LATEX. Since all LATEX field experiments occurred in late summer, the focus has been mainly on stratified conditions. A schematic of the main surface circulation processes that can occur in the western GoL can be found in Fig. 11. This schematic of the surface layer exhibits four main dynamical conditions: (a) retention of water by an eddy; (b) peeling of an eddy into a transient structure and GoL-exiting cross-shelf flux at the southern edge; (c) frontal structure and associated southward fluxes, as during Latex10; and (d) intrusion of a barotropic current on the shelf between the coast and the NC, during

Northwestern wind. The first three cases were encountered during LATEX. The last case was studied numerically but with scarce *in situ* data collected before LATEX (Petrenko et al. 2008).

7 Perspectives

The arrival of the US-French wide-swath altimetry mission SWOT (Surface Water Ocean Topography, scheduled for 2021) will improve the accuracy of the representation of coastal circulation structures and their temporal evolution. Thanks to its Synthetic Aperture Radar (SAR) interferometer, the SWOT satellite will provide precise altimetry measurements close to the coast. SWOT will also increase by an order of magnitude the resolution of 2D maps of sea surface height (SSH). As shown by LATEX modeling and *in situ* activities, coastal eddies and fronts have an important role in modulating cross-shelf exchanges, but due to their potentially small size they are often invisible in SSH images. Therefore, these structures are often detected only indirectly, either by *in situ* techniques—like drifter or glider experiments—or through remote sensing, by their signature in SST or Chl images. The availability of SWOT data will mark a new generation of experiments because it will relieve *in situ* operations from the task of identifying and following in time the fine-scale physical features. Once these features are accessible from remote sensing, *in situ* experiments will have the possibility of concentrating on the characterization of the fine-scale dynamics, using images of high-resolution altimetry for tracking submesoscale features, such as filaments and small eddies. This way, ship-time will be fully available for a proper characterization of the 3D dynamics occurring in between the meso- and the submesoscale, addressing key uncertainties like the quantification of vertical fluxes of nutrient and carbon in frontal systems. In this regard, the Mediterranean sea is set to play a special role; due to its easy accessibility, small Rossby radius, energetic boundary currents, very low cloud coverage, and low tides, it is an ideal “pocket ocean” where to combine high-resolution satellite observations and multi-platform *in situ* experiments. SWOT is expected to resolve features down to 15 km including near the coast. In turn, this information will hopefully improve the realism of circulation models, in particular their representation of biogeochemical processes.

This review concentrated on the physics component of LATEX. Only a short summary is given here on what has been done concerning physical-biogeochemical coupling and the perspectives that this work opens. The LATEX numerical study of the GoL circulation has allowed for the quantification of the impact of the anticyclonic eddy A1_01 on the ecosystem dynamics (Campbell et al. 2013). Additionally, the circulation model Symphonie was coupled

with a biogeochemical model originating from the Eco3M modeling platform (Baklouti et al. 2006a, b), and adapted as a pelagic plankton ecosystem model for the Northwestern Mediterranean basin by Auger et al. (2011). The eddy exhibited low productivity at its core and rising up of nutricline on its edges. However, the functioning and consequences of the coastal eddy on nutrients and plankton distributions were complicated by potential interactions with topography, wind-induced upwelling along the coast and the nearby NC. This coupled modeling is to be pursued to compare the numerical results with the *in situ* data collected during the LATEX cruises (F. Diaz, LATEX PI for biogeochemistry; pers. comm.). More work needs to be done in order to estimate not only the impacts of LATEX eddies on biogeochemical budgets and cross-shelf transfers, but also to comprehend the coupling of physics and biogeochemistry at (sub)mesoscale in this zone.

The LATEX adaptive real-time Lagrangian strategy needs also to be accompanied with 3D *in situ* observations and fast, automated physical and biogeochemical sampling in order, among others, to explore surface semi-geostrophic model (Badin 2013) and to study processes associated with eddies, fronts and filaments (e.g., frontogenesis/frontolysis as in Hoskins (1982)), as well as coupled physical-biogeochemical processes at the submesoscale. This challenge was already highlighted in the open ocean (Lévy et al. 2012) and remains highly relevant in the coastal environment.

8 Availability of the LATEX and SPASSO codes

The LATEXtools software (Doglioli et al. 2013) is written in Matlab and is available freely on the LATEX web site: <http://www.mio.univ-amu.fr/LATEX>. To our knowledge, no other papers report detailed descriptions of the techniques and software adopted for Lagrangian tracer release and sampling strategy, although they are a key point for the success of *in situ* tracer experiments. We are nonetheless aware of the now available Google Earth interactive map of the LatMix project doi:(10.1175/BAMS-D-14-00015.2). Since 2010, the LATEX Lagrangian strategy has been further developed and successfully applied during several other ocean campaigns such as KEOPS2 in 2011 (Quéguiner 2011; d’Ovidio et al. 2015), STRASSE in 2012 (Reverdin et al. 2015) and, in 2015, OUTPACE (Moutin and Bonnet 2015) and OSC-AHR (Doglioli 2015). In the continuity of LATEXtools, SPASSO (Software Package for an Adaptive Satellite-based Sampling for Ocean campaigns, available at <http://www.mio.univ-amu.fr/SPASSO>) retrieves and processes satellite data on land and then transmits them on board. The analysis of the collected information (including *in situ* data and

available model predictions, in addition to the satellite data) is done on land and allows to prepare daily bulletins with suggestions for optimal ship routing and station positioning. These bulletins are then send on board, as well as made available through dedicated web pages. SPASSO is planned to be used for the cruises PEACETIME (2017, PIs: C. Guieu and K. Desboeufs), SARGASSES (2017, PIs: L. Berline and T. Thibaut), and BIOSWOT (2018, PI: F. d'Ovidio).

Acknowledgments The LATEX project was supported by the programs LEFE/IDAO and LEFE/CYBER of the INSU-Institut National des Sciences de l'Univers and by the Region PACA-Provence Alpes Côte d'Azur. The PIs of the project were A. Petrenko for the physics component and F. Diaz for the biogeochemical component. The chief scientists were A. Petrenko on board the *R/V Téthys II* for Latex00, Latex07, Latex08, Latex09, and Latex10 and B. Quéguiner on board the *R/V Le Suroît* for Latex10. The scientist in charge of the tracer release was S. Blain. M. Kersalé and Z.Y. Hu were financed by MENRT Ph.D. grants. F.Nencioli acknowledges support from the FP7 Marie Curie Actions of the European Commission, via the Intra-European Fellowship (FP7-PEOPLE-IEF-2011), project "Lyapunov Analysis in the COaSTal Environment" (LACOSTE-299834). We thank I. Dekeyser for his support and useful discussions. We have appreciated that Claude Estournel and Patrick Marsaleix provided us the initial Symphonie code and helped us along our configuration development. We acknowledge the MFSTEP program for OGCM outputs. Meteorological and AVHRR data were supplied by Météo-France. The DT-INSU is thanked for the treatment of the thermosalinograph data. The altimeter products were produced by Ssalto/Duacs and distributed by Aviso with support from CNES, that also financed the post-doc fellowship of Jérôme Bouffard. The MODIS Aqua data were supplied by the Distributed Active Archive Center at NASA Goddard Space Flight Center and made possible by the MODIS Project. We thank the crews and technicians of the *R/V Le Suroît* and the *R/V Téthys II*, the DT-INSU and all the LATEX collaborators for their assistance at sea or during the project. A special thanks goes to, in alphabetical order, Anne Desnues, Jean-Luc Fuda, Nicolas Grima, Thierry Labasque, Deny Malengros, Peggy Rimmelin, Gilles Rougier, and Anna Roumyantseva, for their work on the data collection and Lagrangian strategy, as well as Emmanuel Bosc for some chlorophyll-a satellite products.

References

- Abraham E, Law C, Boyd P, Lavender S, Maldonado M, Bowie A (2000) Importance of stirring in the development of an iron-fertilized phytoplankton bloom. *Nature* 407:727–730
- Allou A, Forget P, Devenon JL (2010) Submesoscale vortex structures at the entrance of the Gulf of Lions in the Northwestern Mediterranean Sea. *Cont Shelf Res* 30:724–732
- Auger PA, Diaz F, Ulses C, Estournel C, Neveux J, Joux F, Pujopay M, Naudin JJ (2011) Functioning of the planktonic ecosystem of the Rhone River plume (NW Mediterranean) during spring and its impact on the carbon export: a field data and 3-D modelling combined approach. *Biogeosciences* 24(6):9039–9116
- Aurell E, Boffetta G, Crisanti A, Paladin G, Vulpiani A (1997) Predictability in the large: an extension of the concept of Lyapunov exponent. *J Phys A* 30(1):1
- Badin G (2013) Surface semi-geostrophic dynamics in the ocean. *Geophys Astrophys Fluid Dyn* 107(5):526–540
- Baklouti M, Diaz F, Pinazo C, Faure V, Quéguiner B (2006a) Investigation of mechanistic formulations depicting phytoplankton dynamics for models of marine pelagic ecosystems and description of a new model. *Prog Oceanogr* 71(1):1–33
- Baklouti M, Faure V, Pawlowski L, Sciandra A (2006b) Investigation and sensitivity analysis of a mechanistic phytoplankton model implemented in a new modular numerical tool (eco3m) dedicated to biogeochemical modelling. *Prog Oceanogr* 71(1):34–58
- Barrier N, Petrenko AA, Ourmières Y (2016) Strong intrusions of the Northern Mediterranean Current on the eastern Gulf of Lion: insights from *in-situ* observations and high resolution numerical modelling. *Ocean Dyn* 66(3):313–327
- Bauer JE, Druffel ERM (1998) Ocean margins as a significant source of organic matter to the deep open ocean. *Nature* 392:482–485
- Beron Vera FJ, Olascoaga MJ, Goni GJ (2008) Oceanic mesoscale eddies as revealed by Lagrangian coherent structures. *Geophys Res Lett* 35(12)
- Biscaye PE (1994) Shelf edge exchange processes in the southern middle atlantic bight: Seep-ii. *Deep-Sea Res* 41(2-3):229–230
- Bosse A, Testor P, Houpert L, Damien P, Prieur L, Hayes D, Tailandier V, Durrieu de Madron X, d'Ortenzio F, Coppola L, Karstensen J, Mortier L (2016) Scales and dynamics of submesoscale coherent vortices formed by deep convection in the northwestern mediterranean sea. *J Geophys Res* 121(10):7716–7742
- Bouffard J, Nencioli F, Escudier R, Doglioli AM, Petrenko AA, Pascual A, Poulain PM, Elhmaidi D (2014) Lagrangian analysis of satellite-derived currents: application to the North Western Mediterranean coastal dynamics. *Adv Space Res* 53(5):788–801
- Bouffard J, Vignudelli S, Herrmann M, Lyard F, Marsaleix P, Ménard Y, Cipollini P (2008) Comparison of ocean dynamics with a regional circulation model and improved altimetry in the Northwestern Mediterranean. In: *Terr. Atmos. Ocean. Sci.*, vol 19, pp 117–133
- Brink KH, Cowles TJ (1991) The Coastal Transition Zone program. *J Geophys Res* 96(C8):14637–14647
- Broche P, Devenon J-L, Forget P, de Maistre J-C, Naudin J-J, Cauwet G (1998) Experimental study of the Rhone plume. Part I: physics and dynamics. *Oceanol Acta* 21(6):725–738
- Burchard H, Burchard R (2008) A dynamic equation for the potential energy anomaly for analysing mixing and stratification in estuaries and coastal seas. *Estuar Coast Shelf Sci* 77(4):679–687
- Burchard H, Craig PD, Gemmrich JR, van Haren H, Mathieu P-P, Meier HM, Smith WAMN, Prandke H, Rippeth TP, Skillingstad ED et al (2008) Observational and numerical modeling methods for quantifying coastal ocean turbulence and mixing. *J Phys Oceanogr* 76(4):399–442
- Campbell RFD, Hu Z, Doglioli A, Petrenko A, Dekeyser I (2013) Nutrients and plankton spatial distributions induced by a coastal eddy in the Gulf of Lion. Insights from a numerical model. *Prog Oceanogr* 109:47–69
- Canals M, Puig P, de Madron XD, Heussner S, Palanques A, Fabres J (2006) Flushing submarine canyons. *Nature* 444(7117):354–7
- Capet X, McWilliams J, Molemaker M, Shchepetkin A (2008a) Mesoscale to submesoscale transition in the California Current System. Part I: Flow structure, eddy flux, and observational tests. *J Phys Oceanogr* 38(1):29–43
- Capet X, McWilliams JC, Molemaker MJ, Shchepetkin A (2008b) Mesoscale to submesoscale transition in the California Current System. Part II: Frontal processes. *J Phys Oceanogr* 38(1):44–64
- Costa A, Doglioli A, Marsaleix P, Petrenko A (2016) Comparison of *in situ* microstructure measurements to different turbulence closure schemes in a 3-D numerical ocean circulation model. *Ocean Model*, (submitted)
- Cotté C, d'Ovidio F, Chaigneau A, Lévy M, Taupier Letage I, Mate B, Guinet C (2011) Scale-dependent interactions of Mediterranean

- whales with marine dynamics. *Limnol Oceanogr* 106(20):219–232
- Crawford WR (2002) Physical characteristics of Haida Eddies. *J Oceanogr* 58(5):703–713
- Csanady G (1982) Circulation in the coastal ocean. D.Reidel Publishing Company Kluwer Group. Dordrech, Holland
- Cushman-Roisin B (1994) Introduction to geophysical fluid dynamics. Prentice Hall
- De Boer GJ, Pietrzak JD, Winterwerp JC (2008) Using the potential energy anomaly equation to investigate tidal straining and advection of stratification in a region of freshwater influence. *Ocean Model* 22:1–11
- De Monte S, D'Ovidio F, Cotté C, Lévy M, Le Corre M, Weimerskirch (2012) Frigatebird behaviour at the ocean-atmosphere interface: integrating animal behaviour with multisatellite data. *J. R. Soc. Interface*
- Di Lorenzo E, Foreman MGG, Crawford WR (2005) Modelling the generation of Haida Eddies. *Deep-Sea Res II* 52:853–873
- Doglioli A (2015) OSCAHR cruise, RV *Téthys II*, doi:10.17600/15008800
- Doglioli A, Nencioli F, Petrenko AA, Fuda J-L, Rougier G, Grima N (2013) A software package and hardware tools for *in situ* experiments in a Lagrangian reference frame. *J Atmos Ocean Tech* 30(8)
- Doglioli AM, Blanke B, Speich S, Lapeyre G (2007) Tracking coherent structures in a regional ocean model with wavelet analysis: application to Cape Basin Eddies. *J Geophys Res* 112
- d'Ovidio F, De Monte S, Alvain S, Dandonneau Y, Lévy M (2010) Fluid dynamical niches of phytoplankton types. *Proc Natl Acad Sci USA* 107(43):18366–18370
- d'Ovidio F, Della Penna A, Trull TW, Nencioli F, Pujol M-I, Rio M-H, Park Y-H, Cotté C, Zhou M, Blain S (2015) The biogeochemical structuring role of horizontal stirring: Lagrangian perspectives on iron delivery downstream of the Kerguelen Plateau. *Biogeochemistry* 12(19):5567–5581
- d'Ovidio F, Fernández V, Hernández-García E, López C (2004) Mixing structures in the mediterranean sea from finite-size lyapunov exponents. *Geophys Res Lett* 31:L17203
- Durrieu de Madron X, Houpert L, Puig P, Sanchez-Vidal A, Testor P, Bosse A, Estournel C, Somot S, Bourrin F, Bouin MN (2012) Interaction of dense shelf water cascading and open-sea convection in the northwestern mediterranean during winter. *Geophys Res Lett* 40(7):1379–1385
- Durrieu de Madron X, Zervakis V, Theocharis A, Georgopoulos D (2005) Comments on cascades of dense water around the world ocean. *Prog Oceanogr* 64(1):83–90
- Estournel C, Durrieu de Madron X, Marsaleix P, Auclair F, Julliard C, Vehil R (2003) Observation and modeling of the winter coastal oceanic circulation in the Gulf of Lion under wind conditions influenced by the continental orography (FETCH experiment). *J Geophys Res* 108(C3)
- Ferrari R (2011) A frontal challenge for climate models. *Science* 332(6027):316–7
- Filament P, Armi L, Washburn L (1985) The evolving structure of an upwelling filament. *J Geophys Res* 90(C6):11765–11778
- Flexas MM, Durrieu de Madron X, Garcia MA, Canals M, Arnau P (2002) Flow variability in the Gulf of Lions during the MATER HFF experiment (March-May 1997). *J Mar Syst* 33-34:197–214
- Garreau P, Garnier V, Schaeffer A (2011) Eddy resolving modelling of the Gulf of Lions and Catalan Sea. *Ocean Dyn* 61:991–1003
- Gaspar P, Grégoris Y, Lefevre J-M (1990) A simple eddy kinetic energy model for simulations of the oceanic vertical mixing: tests at Station Papa and long-term upper ocean study site. *J Geophys Res* 95:179–193
- Gattuso J-P, Frankignoulle M, Wollast R (1998) Carbon and carbonate metabolism in coastal aquatic ecosystems. *Annu Rev Ecol Syst* 29:405–434
- Grantham BA, Chan F, Nielsen KJ, Fox DS, Barth JA, Huyer A, Lubchenco J, Menge BA (2004) Upwelling-driven nearshore hypoxia signals ecosystem and oceanographic changes in the northeast Pacific. *Nature* 429:749–754
- Griffa A, Kirwan A, Mariano AJ, Özgökmen T, Rossby HT (2007) Lagrangian analysis and prediction of coastal and ocean dynamics. Cambridge University Press
- Gustafsson Ö, Buesseler KO, Geyer WR, Moran SB, Gschwend PM (1998) An assessment of the relative importance of horizontal and vertical transport of particle-reactive chemicals in the coastal ocean. *Cont Shelf Res* 18(7):805–829
- Haller G (2011) A variational theory of hyperbolic Lagrangian Coherent Structures. *Phys D* 240(7):574–598
- Haller G, Yuan G (2000) Lagrangian coherent structures and mixing in two-dimensional turbulence. *Phys D* 147:352–370
- Haza AC, Özgökmen TM, Griffa A, Molcard A, Poulain P-M, Peggion G (2010) Transport properties in small-scale coastal flows: relative dispersion from VHF radar measurements in the Gulf of La Spezia. *Ocean Dyn* 60(4):861–882
- Haza AC, Poje AC, Özgökmen TM, Martin P (2008) Relative dispersion from a high-resolution coastal model of the Adriatic Sea. *Ocean Model* 22(1-2):48–65
- Holtermann PL, Umlauf L, Tanhua T, Schmale O, Rehder G, Waniek JJ (2012) The Baltic Sea Tracer Release Experiment: 1. Mixing rates. *J Geophys Res* 117(C1)
- Hopkins J, Sharples J, Huthnance JM (2012) On-shelf transport of slope water lenses within the seasonal pycnocline. *Geophys Res Lett* 39(8):85–93
- Hoskins B (1982) The mathematical theory of frontogenesis. *Annu Rev Fluid Mech* 14:31–151
- Hu ZY, Doglioli AM, Petrenko AA, Marsaleix P, Dekeyser I (2009) Numerical simulations of eddies in the Gulf of Lion. *Ocean Model* 28(4):203 – 208
- Hu ZY, Petrenko AA, Doglioli AM, Dekeyser I (2011a) Numerical study of eddy generation in the western part of the Gulf of Lion. *J Geophys Res* 116
- Hu ZY, Petrenko AA, Doglioli AM, Dekeyser I (2011b) Study of mesoscale anticyclonic eddy in the western part of the Gulf of Lion. *J Mar Syst* 88:3–11
- Huthnance J (1995) Circulation, exchange and water masses at the ocean margin: the role of physical processes at the shelf edge. *Prog Oceanogr* 35(4):353–431
- Huthnance JM, Holt JT, Wakelin SL (2009) Deep ocean exchange with west-european shelf seas. *Ocean Sci* 5(4):621–634
- Huthnance JM, Van Aken HM, White M, Barton ED, Le Cann B, Ferreira Coelho E, Alvarez Fanjul E, Miller P, Vitorino J (2002) Ocean margin exchange—water flux estimates. *J Mar Syst* 32(1-3):107–137
- Johnson J, Chapman P (2011) Preface Deep Ocean Exchange with the Shelf (DOES). *Ocean Sci* 7(1)
- Kersalé M, Doglioli AM, Petrenko AA, Dekeyser I, Nencioli F (2013) Physical characteristics and dynamics of the coastal Latex09 Eddy derived from *in situ* data and numerical modeling. *J Geophys Res* 118:1–11
- Kersalé M, Petrenko AA, Doglioli AM, Nencioli F, Bouffard J, Blain S, Diaz F, Labasque T, Quéguiner B, Dekeyser I (2015) Lateral diffusivity coefficients from the dynamics of a SF6 patch in a coastal environment. *J Mar Syst* 153:42–54
- Kirincich AR, Barth JA (2009) Time-varying across-shelf ekman transport and vertical eddy viscosity on the inner shelf. *J Phys Oceanogr* 39(3):602
- Law C, Watson A, Liddicoat M (1994) Automated vacuum analysis of sulphur hexafluoride in seawater: derivation of the atmospheric

- trend (1970–1993) and potential as a transient tracer. *Mar Chem* 48(1):57–69
- Ledwell JR, Watson AJ (1991) The Santa-Monica Basin tracer experiment—a study of dyapycnal and isopycnal mixing. *J Geophys Res* 96(C5):8695–8718
- Ledwell JR, Watson AJ, Law CS (1998) Mixing of a tracer in the pycnocline. *J Geophys Res* 103(C10):21499–21529
- Lehahn Y, d'Ovidio F, Lévy M, Heifetz E (2007) Stirring of the northeast atlantic spring bloom: a lagrangian analysis based on multisatellite data. *J Geophys Res* 112(C08005)
- Lévy M., Ferrari R, Franks PJ, Martin AP, Rivière P (2012) Bringing physics to life at the submesoscale. *Geophys. Res. Lett.*, 39(14)
- Lumpkin R, Elipot S (2010) Surface drifter pair spreading in the North Atlantic. *J Geophys Res* 115
- MacFadyen A, Hickey BM (2010) Generation and evolution of a topographically linked, mesoscale eddy under steady and variable wind-forcing. *Cont Shelf Res* 30(13):1387–1402
- MacFadyen A, Hickey BM, Cochlan WP (2008) Influences of the Juan de Fuca Eddy on circulation, nutrients, and phytoplankton production in the northern California Current System. *J Geophys Res* 113(C08008)
- Mahadevan A (2016) The impact of submesoscale physics on primary productivity of plankton. *Ann Rev Mar Sci* 8(1):161–184
- Mancho AM, Hernandez Garcia E, Small D, Wiggins S, Fernandez V (2008) Lagrangian transport through an ocean front in the north-western Mediterranean sea. *J Phys Oceanogr* 38(6):1222–1237
- Marsaleix P, Auclair F, Estournel C (2006) Considerations on open boundary conditions for regional and coastal ocean models. *J Atmos Ocean Technol* 23:1604–1613
- Marsaleix P, Auclair F, Floor J, Herrmann M, Estournel C, Pairaud I, Ulses C (2008) Energy conservation issues in sigma-coordinate free-surface ocean models. *Ocean Model* 20:61–89
- McWilliams JC, Brown ED, Bryden HL, Ebbesmeyer CC, Elliott BA, Heinmiller RH, Lien Hua B, Leaman KD, Lindstrom EJ, Luyten JR, McDowell SE, Breckner Owens W, Perkins H, Price JF, Regier L, Riser SC, Rossby HT, Sanford TB, Shen CY, Taft BA, Van Leer JC (1983) The local dynamics of Eddies in the Western North atlantic. Springer Berlin Heidelberg, Berlin, Heidelberg, pp 92–113
- Melson A, Meyers SD, Hurlburt HE, Metzger EJ, O'Brien JJ (1999) ENSO effects on Gulf of Alaska eddies. *Earth Interact* 3:003
- Millot C (1979) Wind induced upwellings in the Gulf of Lions. *Oceanol Acta* 2:261–274
- Millot C (1982) Analysis of upwelling in the Gulf of Lions—hydrodynamics of semi-enclosed seas: Proceedings of the 13th International liège Colloquium on Ocean Hydrodynamics, vol 34. Elsevier Oceanogr. Ser. Amsterdam, The Netherlands
- Millot C (1990) The Gulf of Lions' hydrodynamics. *Cont Shelf Res* 10:885–894
- Millot C, Crépon M (1981) Inertial oscillations on the continental shelf of the Gulf of Lions. *J Phys Oceanogr* 11:639–657
- Millot C, Taupier-Letage I (2005) Additional evidence of LIW entrainment across the Algerian subbasin by mesoscale eddies and not by a permanent westward flow. *Prog Oceanogr* 66(2):231–250
- Millot C, Wald L (1980) The effect of Mistral wind on the Ligurian current near Provence. *Oceanol Acta* 3(4):399–402
- Mitchelson-Jacob G, Sundby S (2001) Eddies of Vestfjorden, Norway. *Cont Shelf Res* 21(16-17):1901–1918
- Moore II T, Matear R, Marra J, Clementson L (2007) Phytoplankton variability off the western australian coast: mesoscale eddies and their role in cross-shelf exchange. *Deep-Sea Res II* 54(8-10):943–960
- Moutin T, Bonnet S (2015) OUTPACE cruise, RV L'Atalante. doi:10.17600/15000900
- Nagai T, Gruber N, Frenzel H, Lachkar Z, McWilliams JC, Plattner G-K (2015) Dominant Role of Eddies and Filaments in the Offshore Transport of Carbon and Nutrients in the California Current System. *J Geophys Res* 120
- Naudin JJ, Cauwet G, Chretiennot-Dinet M-J, Deniaux B, Devenon J-L, Pauc H (1997) River discharge and wind influence upon particulate transfer at the land–ocean interaction: case study of the Rhône river plume. *Estuar Coast Shelf Sci* 45(3):303–316
- Nencioli F, d'Ovidio F, Doglioli A, Petrenko A (2013) *In situ* estimates of submesoscale horizontal eddy diffusivity across an ocean front. *J Geophys Res* 118(12):7066–7080
- Nencioli F, d'Ovidio F, Doglioli AM, Petrenko AA (2011) Surface coastal circulation patterns by *in-situ* detection of Lagrangian coherent structures. *Geophys Res Lett* 38(L17604)
- Nencioli F, Kuwahara VS, Dickey TD, Rii YM, Bidigare RR (2008) Physical dynamics and biological implications of a mesoscale eddy in the lee of Hawai'i : Cyclone Opal observations during E-FLUX III. *Deep-Sea Res II* 55(10-13):1252–1274
- Nencioli F, Petrenko AA, Doglioli AM (2016) Diagnosing cross-shelf transport along an ocean front: an observational case study in the Gulf of Lion. *J Geophys Res* (121):7218–7243
- Nof D (1999) Strange encounters of eddies with walls. *J Mar Res* 57(5):739–761
- Olascoaga MJ, Rypina II, Brown MG, Beron Vera FJ, Kocak H, Brand LE, Halliwell GR, Shay LK (2006) Persistent transport barrier on the West Florida Shelf. *Geophys Res Lett* 33(22)
- Petrenko AA (2003) Variability of circulation features in the Gulf of Lion NW Mediterranean Sea. Importance of inertial currents. *Oceanol Acta* 26:323–338
- Petrenko AA (2007) Latex00 cruise in the Gulf of Lion, RV Thélys II, doi:10.17600/7450130
- Petrenko AA (2008) Latex08 cruise in the Gulf of Lion, RV Thélys II, doi:10.17600/8450140
- Petrenko AA (2009) Latex09 cruise in the Gulf of Lion, RV Thélys II, doi:10.17600/9450140
- Petrenko AA (2010) Latex10 cruise in the Gulf of Lion, RV Thélys II, doi:10.17600/10450150
- Petrenko AA, Dufau C, Estournel C (2008) Barotropic eastward currents in the western Gulf of Lion, northwestern Mediterranean Sea, during stratified conditions. *J Mar Syst* 74(1-2):406–428
- Petrenko AA, Kersalé M, Nencioli F, Gatti J, Doglioli AM, Dekeyser I (2013) Coastal circulation in the Gulf of Lion, the influence of mesoscale processes on interregional exchanges. 40th CIESM Congress proceedings
- Petrenko AA, Leredde Y, Marsaleix P (2005) Circulation in a stratified and wind-forced Gulf of Lions, NW Mediterranean Sea: *in situ* and modeling data. *Cont Shelf Res* 25:7–27
- Pinardi N (2003) The Mediterranean ocean forecasting system : first phase of implementation (1998-2001). *Ann Geophys* 21:3–20
- Quéguiner B (2011) KEOPS 2 cruise, RV Marion Dufresne, doi:10.17600/11200050
- Reverdin G, Morisset S, Marié L, Bourras D, Sutherland G, Ward B, Salvador J, Font J, Cuypers Y, Centurioni L, Hormann V, Koldziejczyk N, Boutin J, D'Ovidio F, Nencioli F, Martin N, Diverres D, Alory G, Lumpkin R (2015) Surface salinity in the North Atlantic subtropical gyre during the STRASSE/SPURS summer 2012 cruise. *Oceanography* 28:114–123
- Robinson AR (1983) Overview and summary of Eddy science. Springer Berlin Heidelberg, Berlin, Heidelberg, pp 3–15
- Roughan M, Garfield N, Largier J, Dever E, Dorman C, Peterson D, Dorman J (2006) Transport and retention in an upwelling region: the role of across-shelf structure. *Deep-Sea Res II* 53(25–26):2931–2955
- Ruiz S, Pascual A, Mahadevan A, Claret M, Olita A, Troupin C, Tintoré J, Poulain P, Tovar-Sánchez A, Mourre B, Capet A (2016) Intense ocean frontogenesis inducing submesoscale processes and impacting biochemistry 48th International liège Colloquium on Ocean Dynamics, Liège, Belgium. oral pres

- Schaeffer A, Molcard A, Forget P, Fraunié P, Garreau P (2011) Generation mechanisms for mesoscale eddies in the Gulf of Lions : radar observation and modeling. *Ocean Dyn* 61:1587–1609
- Schroeder K, Haza AC, Griffa A, Özgökmen TM, Poulain P, Gerin R, Peggion G, Rixen M (2011) Relative dispersion in the Liguro-Provencal basin: from sub-mesoscale to mesoscale. *Deep-Sea Res I* 58(3):209–228
- Shcherbina AY, Sundermeyer MA, Kunze E, D’Asaro E, Badin G, Birch D, Brunner-Suzuki A-MEG, Callies J, Kuebel Cervantes BT, Claret M, Concannon B, Early J, Ferrari R, Goodman L, Harcourt RR, Klymak JM, Lee CM, Lelong M-P, Levine MD, Lien R-C, Mahadevan A, McWilliams JC, Molemaker MJ, Mukherjee S, Nash JD, Özgökmen T, Pierce SD, Ramachandran S, Samelson RM, Sanford TB, Shearman RK, Skillingstad ED, Smith KS, Tandon A, Taylor JR, Terray EA, Thomas LN, Ledwell JR (2015) The LatMix Summer Campaign: Submesoscale Stirring in the Upper Ocean. *Bull Am Meteorol Soc* 96(8):1257–1279
- Ssalto/Duacs User Handbook CNES (2010) (M)SLA and (M)ADT near-real time and delayed time products, CNES (Centre National d-Etudes Spatiales). Technical report. Ref. cLS-DOS-NT-06.034
- Staneva JV, Dietrich DE, Stanev EV, Bowman MJ (2001) Rim current and coastal eddy mechanisms in an eddy-resolving Black Sea general circulation model. *J Mar Syst* 31(1):137–157
- Suthers IM, Young JW, Baird ME, Roughan M, Everett JD, Brassington GB, Byrne M, Condie SA, Hartog JR, Hassler CS (2011) The strengthening East Australian Current, its eddies and biological effects—an introduction and overview. *Deep-Sea Res II* 58(5):538–546
- Tew Kai E, Rossi V, Sudre J, Weimerskirch H, Lopez C, Hernandez Garcia E, Marsac F, Garçon V (2009) Top marine predators track Lagrangian coherent structures. *Proc Natl Acad Sci USA* 106(20):8245–8250
- Thomas LN, Tandon A, Mahadevan A (2008) Submesoscale processes and dynamics. *American Geophysical Union*, pp 17–38
- Wanninkhof R, Hitchcock G, Wiseman WJ, Vargo G, Ortner PB, Asher W, Ho DT, Schlosser P, Dickson M-L, Masserini R et al (1997) Gas exchange, dispersion, and biological productivity on the west Florida shelf: results from a Lagrangian tracer study. *Geophys Res Lett* 24(14):1767–1770
- Waugh DW, Abraham E (2008) Stirring in the global surface ocean. *Geophys Res Lett* 35(20)